

Transition Modeling in Support of CFD Vision 2030 – Highlights of Recent Efforts at the NASA Langley Research Center

Meelan Choudhari¹, Ethan Beyak¹, Nathaniel Hildebrand¹, Fei Li¹, Ethan Vogel¹, Pedro Paredes², Vishal Srivastava³ & Balaji Venkatachari³

Abstract

CFD Vision 2030 has identified the prediction of viscous turbulent flows with transition and separation as a critical pacing item for CFD simulation capability. To address the requirements for transition modeling integrated with CFD, NASA Langley Research Center has adopted a dual strategy that seeks to enhance the robustness of automated stability computations coupled with RANS solvers as well as improving the accuracy and range of applicability of transition models based on auxiliary transport equations. This paper outlines the implementation and evaluation of both approaches in NASA flow solvers. The assessment includes 2D and 3D boundary layers with various pressure gradients, edge Mach numbers, and multiple instability mechanisms that may lead to transition, either in isolation or in concert with one another. Furthermore, the development of machine-learning-based stability models as an effective surrogate for direct computation of instability characteristics is outlined. Several shortcomings of current transport-equation-based models have been identified. These include inadequate physics to capture the effects of disturbance growth history, compressibility effects at high subsonic through hypersonic speeds, limitations of roughness-sensitized crossflow models, and the failure to account for the effects of local geometric perturbations like step excrescences. The paper suggests improvements to address some of these challenges and highlights recent advances in transition model verification and design optimization for laminar flow technology.

Keywords: Computational Fluid Dynamics, Laminar-Turbulent Transition, Hydrodynamic Instability

1. Introduction

According to the CFD Vision 2030 [1], a major challenge in computational fluid dynamics (CFD) simulations pertains to the accurate prediction of viscous flows with laminar-turbulent transition and flow separation. Modeling (rather than resolving) transition has also been identified as an enabler to substantial reductions in cost for eddy-resolved simulations of high Reynolds flows such as those over transport aircraft wings. A majority of stationary CFD computations assume fully turbulent flow, which allows one to use the computationally efficient and generally robust framework of Reynolds-averaged Navier-Stokes (RANS)-based turbulence models throughout the flowfield. However, neglect of transition can lead to significant errors in predicting the performance metrics in a number of applications, including aerodynamic designs with natural laminar flow (NLF) technology, high-lift configurations, rotorcraft flows, and unmanned aerial vehicles. Different turbulence models have their own intrinsic transition behavior, but they cannot fully capture the complex physics of the actual transition process.

Semiempirical transition correlations based on linear stability theory (LST), such as the e^N or the N-factor method introduced by Smith and Gamberoni [2] and van Ingen [3], are widely used for predicting the onset of transition. Even though the N-factor approach does not explicitly model the intricate details of the receptivity process or the nonlinear stages of transition, it has been found to provide reasonable predictions of transition locations and/or associated trends in a broad class of

¹ NASA Langley Research Center, Hampton, VA 23681

² National Institute of Aerospace, Hampton, VA 23666

³ Analytical Mechanics Associates, Hampton, VA 23666

[§] The order of coauthors is alphabetical and does not signify their individual contributions

boundary layer flows across the speed regime. However, automated direct computations of stability characteristics tend to suffer from a lack of robustness and often require significant user expertise. This shortcoming can be alleviated via surrogate models for N-factor computation [4–8]. However, stability-based transition modeling intrinsically relies upon multiple forms of nonlocal flow information and requires supplementary models for the transition zone. These limitations reduce their appeal in the context of parallel CFD computations, especially with unstructured grids.

The alternate approach of supplementing the turbulence model equations in RANS CFD with additional transport equations can predict both the onset of transition and the ensuing evolution of intermittency. A notable advance in this area was Menter's introduction of the local correlation-based transition models (LCTMs) [9] that combine local flow variables and empirical correlations to predict the transition region. Designed to couple with Menter's shear stress transport (SST) turbulence model [10], the two-equation Langtry-Menter $\gamma - Re_{\theta t}$ model (LM2009) [11] can predict selected transition mechanisms in quasi-2D flows by solving transport equations for the intermittency γ and a transition criterion $Re_{\theta r}$. The latter is based on the momentum thickness Reynolds number Re_{θ} , which is estimated using a local vorticity-based Reynolds number. Other notable models based on transport equations include Menter et al.'s single-equation γ model [12], the $k-k_l-\omega$ model that includes an equation for the pre-transitional laminar kinetic energy k_l to predict transition without using empirical transition-onset correlations [13] and the Spalart-Allmaras (SA) [14] based amplification factor transport (AFT) model by Coder and Maughmer [15] that incorporates the instability mechanisms underlying transition in a low disturbance environment by modeling the N-factor evolution via a transport equation. Since then, several extensions of these models have been proposed in an attempt to improve accuracy and extend their generality, e.g., to predict crossflow transition in swept-wing boundary layers [16] and second-mode transition in high-speed flows [18-21].

Following the Transition Prediction Workshop in 2017 by NASA,¹ a significant expansion of the transition modeling capabilities in selected NASA flow solvers was undertaken to address the needs highlighted by the CFD Vision 2030 study. This paper presents an overview of this research effort, outlines the key lessons learned, and offers an assessment of the current transition modeling capabilities in the OVERFLOW [22] and FUN3D [23] codes. Recently, key elements of this capability have also been ported to the VULCAN-CFD code [24]. The paper is structured as follows. Section 2 outlines the overall research strategy. Sections 3 and 4 present selected case studies pertinent to the demonstration and assessment of this capability. Section 5 provides concluding remarks. While this overview paper focuses on the work performed at NASA Langley, transition modeling has been an active area of research worldwide [25,26] and numerous related references can be found in the papers cited herein.

2. Overview of Transition Modeling Capabilities

This section describes the research strategy we have adopted for transition model development, which is followed by an overview of the current capabilities implemented in NASA's OVERFLOW and FUN3D codes.

2.1 Research Strategy

Transition represents the response of a deterministic, large degree-of-freedom system to forcing from external disturbances that may be either deterministic and/or stochastic in nature. Whereas turbulence denotes the statistically robust and path-insensitive attractor that denotes the final outcome of this response, transition is all about the myriad pathways through which the flow may reach that outcome. So, an intrinsic challenge in engineering predictions is to account for the diversity of transition mechanisms and their sensitivity to the specific details of the external disturbances. A telltale example of this sensitivity is the experiments by Saric's group [27] at the Texas A&M University, which showed how polishing a painted leading edge of the swept wing pushed back the onset of crossflow transition from 30% to 80% chord. Similarly, transition on hypersonic reentry vehicles is often caused by surface roughness, which may be created (and also modified) in the course of flight. Ground-to-flight extrapolation is often constrained by the large variations in transition associated with unsteady tunnel disturbances. Incorporating such dependencies via a practical set of input parameters is a challenge for both classes of transition models. In contrast, the external disturbances can often be considered as secondary in turbulence modeling.

¹ https://turbmodels.larc.nasa.gov/transition_workshop2017.html

Desirable attributes of transition models for modern and general purpose CFD solvers include accuracy, efficiency, robustness, as well as the ability to work with unstructured grid codes and various turbulence models. CFD Vision 2030 [1] has emphasized physics-based predictive modeling and a higher degree of automation in all steps of the CFD analysis process. This requires transition analysis that is integrated into the CFD solvers, ranging from the steady RANS approach to various forms of eddy-resolving methods. The CFD Vision 2030 Study report also emphasized the need for rigorous verification and validation (V&V) and uncertainty quantification (UQ) practices in the broader context of CFD simulations. This also applies in the specific context of transition modeling, given the complex, multiscale, and sensitive nature of the transition process. With that backdrop, an eventual goal would be to achieve more reliable transition modeling for aerospace applications — across the speed regime, vehicle classes, and their operational envelopes. To facilitate that mission, we have pursued a dual transition modeling strategy based on both stability-based and transport-equations-based paradigms (see Fig. 1). A hierarchy of models with different fidelities is included within each model category to allow users to tackle a broad spectrum of aerospace applications, spanning varying degrees of transition significance to the metrics of interest and the particular goals of CFD analysis. The dual approach expands the coverage of the 2D parameter space shown in Fig. 1 while also enabling the use of stability-based models to guide the assessment and improvement of the LCTMs. The eventual aim is to cross-pollinate between the two classes of models to help incorporate the several attributes mentioned earlier.

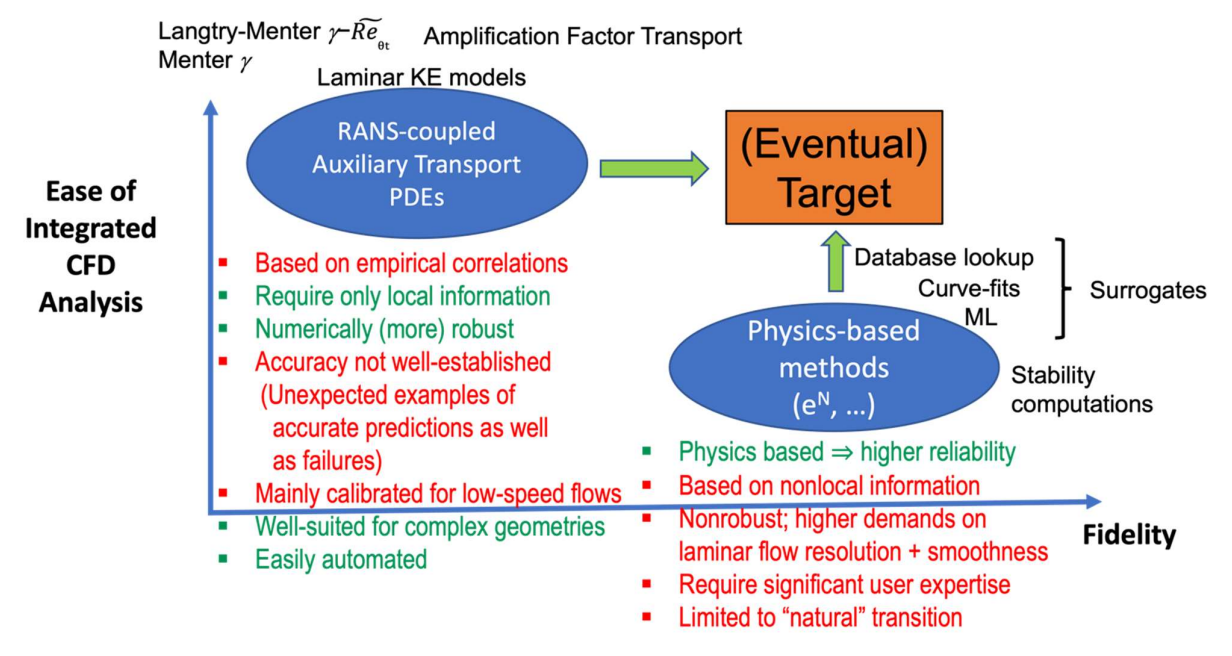


Figure 1 - Dual strategy for CFD integrated transition modeling in NASA flow solvers OVERFLOW and FUN3D.

2.2 Stability-Based Transition Modeling

The modular framework for CFD-integrated transition modeling in Fig. 2 enhances portability across multiple flow solvers as well as a hierarchy of models for N-factor computation. The three main components include: the CFD process (i.e., flow solver and auxiliary tools for pre- and post-processing), a stability solver (stability code or a surrogate model with utilities for N-factor computations along integration trajectories spanning the model surface), and a solver independent module that handles the generic tasks related to the communication between the CFD process and the stability solver.

To ensure a flexible capability that is compatible with multiple flow solvers, we have focused on both a structured, overset grid flow solver (OVERFLOW v. 2.3) and the FUN3D suite (FUN3D, v. 14) that can be used with several mesh formats, including mixed-element unstructured grids and structured multiblock grids with one-to-one interfaces or overset grid systems.

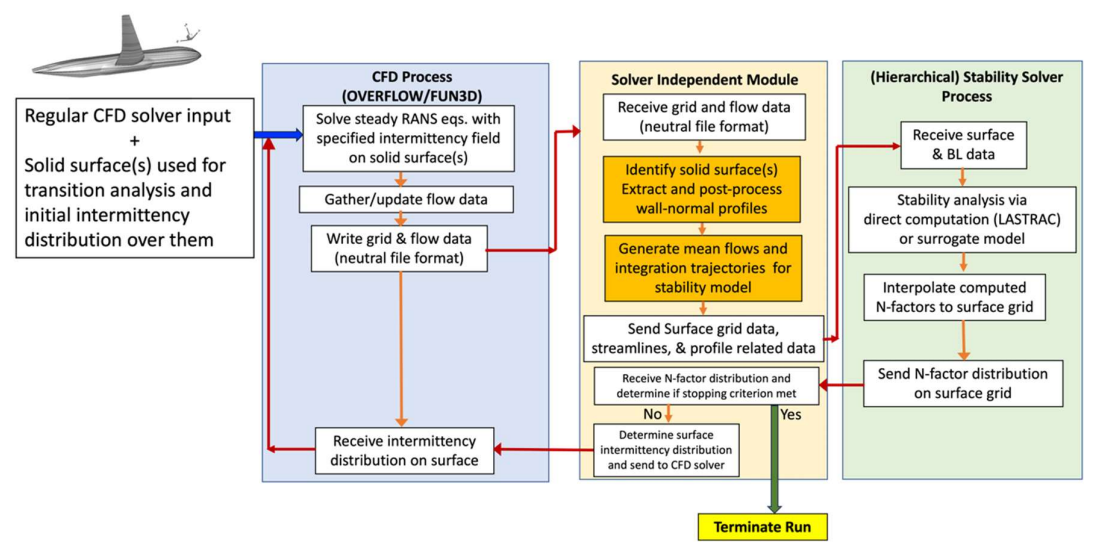


Figure 2 – Computational framework for stability-based transition modeling.

Direct computation of the stability characteristics utilizes the suite of LAngley Stability and TRansition Analysis Codes (LASTRAC) [28,29]. Significant progress has recently been made in improving the automation of stability-based transition modeling [30], including the development of surrogate models derived from deep learning algorithms [31–33]. A majority of this work has been carried out in support of NASA's Transformational Tools and Technologies project, while a significant portion of the model development for high-speed flows has been in support of the Hypersonic Technology project.

The LASTRAC stability solver offers a hierarchy of models that predict disturbance growth based on varying degrees of physical approximations. The LST equations, derived from the linearized Navier-Stokes equations, track the growth of small-amplitude, fixed-frequency disturbances assuming locally parallel mean flow. The Parabolized Stability Equations (PSE) [34] involve fewer assumptions and can account for weakly nonparallel basic state effects, surface geometry curvatures, and a large subset of nonlinear modal interactions. However, only the linear form of PSE has been used for CFD integrated transition modeling described in this paper. Both LST and PSE can model the amplification of primary instabilities on aircraft wings, such as Tollmien-Schlichting (TS) waves and crossflow (CF) vortices. Surface curvature can exert a stronger effect on the disturbance growth of CF instability, and the stabilizing influence of convex curvature on aircraft wings is frequently offset by comparable destabilization due to nonparallel effects. Thus, low-fidelity stability prediction based on the classical, quasiparallel LST often provides sufficiently accurate N-factor predictions. However, for certain configurations, especially designed for natural laminar flow on the wings of subsonic transports, the effects of surface curvature can be significant [35]. In such cases, PSE analysis is required to accurately estimate the contributions of both surface curvature and the nonparallel mean flow. The work by Halila et al. [36] is noteworthy for demonstrating the CFD integration of PSE into a high-order discontinuous Galerkin flow solver for 2D flows. The LASTRAC-based CFD integration, however, is more versatile, and applies to both 2D and fully 3D flows. Nonetheless, the LASTRAC applications described herein are limited to line-marching PSE solutions along specified integration trajectories. Mean-flow inhomogeneities such as streamwise elongated streaks in hypersonic flow configurations require plane-marching PSE for stability predictions. The integration of line- and plane-marching PSE for composite N-factor predictions was considered by Li et al. [37].

The inclusion of stability-based predictions of transition onset alone into RANS or other simulations can sometimes provide adequate estimates of overall flow metrics such as the drag or total heat load. However, accounting for the details of the transition zone may also be necessary to minimize the upstream influence due to abrupt transition associated with binary intermittency in the numerical model, and to reduce the error in integrated loads when the breakdown region is significantly long. As a result, variable fidelity modeling also becomes desirable for the prediction of intermittency evolution across the transition zone. The solver independent module includes different options for intermittency evolution ranging from abrupt transition (binary switch) to algebraic models

based on empirical correlations for a finite length transition zone. This module is comprised of the PyLASTRAC suite of Python codes and a partial description of those codes is provided in Ref. [30].

2.3 Transport-Equations-Based Transition Modeling

The OVERFLOW and FUN3D capabilities for transport-equations-based transition modeling have been augmented via the inclusion of several additional models. As mentioned previously, transport-based models are less general. Therefore the broader range of models adds robustness and also provides an element of uncertainty quantification. Additional benefits of these enhancements include models with Galilean invariance, models that are compatible with additional turbulence models, particularly SA, models with a reduced number of user inputs in some cases, compressibility corrections to improve accuracy at O(1) Mach numbers and above, and the ability to handle a wider range of transition scenarios including second-mode and crossflow transition in hypersonic flows. Table 1 presents a summary of the transition models currently implemented in the OVERFLOW and FUN3D codes.

Table 1. Transport-Equations-Based Transition Models in OVERFLOW and FUN3D (Turbulence model SST2003 refers to Menter's shear stress transport model [10] and SA denotes the Spalart-Allmaras turbulence model [14]. The presence of a check mark in the OVERFLOW and FUN3D columns indicates the availability of a given transition model in that code.)

Turbulence Model	Transition Model	Model Order (Turb- Trans)	OVERFLOW	FUN3D	Remark
SST2003	LM2009	2-2	√	√	Transition due to TS waves , separation bubble, and bypass due to high-amplitude freestream turbulence
SST2003	LM2015	2-2	✓	✓	Includes crossflow, sensitized to surface roughness
SST2003	LM2009- compressibility corrected	2-2	√		Stability-based compressibility correction for subsonic and transonic flows
SST2003	CFHE	2-2	✓	✓	Includes crossflow, no roughness sensitivity
SST2003	Menter γ		✓	✓	Galilean invariant
SST2003	Liu et al. γ		✓		Hypersonic flows, 1st- and 2nd- mode transition and crossflow
SST2003	Qiao et al. $\gamma - \nu_L$		✓		Hypersonic flows, 1st- and 2nd- mode transition and crossflow
SA	Medida-Baeder		✓		
SA	AFT2014	1-1		✓	
SA	AFT2017a	1-1		✓	
SA	AFT2017b	1-2	✓	✓	Galilean invariant
SA	AFT2019	1-2	✓	✓	
SA	LM2015	1-2	√		

3. Case Studies: Stability-Based Transition Modeling

This section outlines the application of stability-coupled transition models from the OVERFLOW and FUN3D solvers to selected flow configurations with prior experimental data. The first two cases (sections 3.1 and 3.2) correspond to swept wing configurations for which attachment line instability does not play a role, but both TS waves and CF instabilities can have appreciable N-factors. In these cases, transition onset is correlated with a front in the two-dimensional space of TS and stationary crossflow N-factors, denoted herein as N_{TS} and N_{CF} , respectively. The shape of this transition boundary in the $N_{TS}-N_{CF}$ space is typically determined through correlation with measurements. For limited consistency, both cases use the same dual N-factor criterion given by:

$$I(N_{TS}, N_{CF}) = \left(\frac{N_{TS}}{N_{TS,c}}\right)^{a_{TS}} + \left(\frac{N_{CF}}{N_{CF,c}}\right)^{a_{CF}} = 1,$$
 (1)

where the subscript c refers to the critical value, and the exponents a_{TS} and a_{CF} control the level of interaction between the two types of instability waves.

3.1 Swept-wing configurations: NASA Juncture Flow Model

The Juncture Flow experiment [38] in the NASA Langley 14- by 22-Foot Subsonic Tunnel provided a valuable opportunity to assess and refine both classes of transition models by augmenting the relatively sparse body of transition measurements for swept wing boundary layers. This experiment employed a top-down symmetric, full-span swept wing configuration based on the NACA-0015 airfoil. It provided mean surface pressure measurements along multiple spanwise stations, along with infrared (IR)-imaging-based transition front measurements on the starboard and port side wings along with the fuselage. As described by Leidy et al. [38], the IR-based transition data on the wing surfaces was consistent with additional transition data derived from mean C_p measurements. The freestream turbulence intensity near the wing leading edge is estimated to be in the range of 0.070% to 0.096%. Additionally, the surface roughness on the painted wings was measured both before and during the experiment.

Figure 3 illustrates the comparison between the predicted Cp distributions along four selected cuts and the corresponding measured data from [38] at two different angles of attack (α = 0° and α = 5°). The close agreement between the two sets of results boosts confidence that the computed laminar flow mimics the boundary layer evolution in the experiment, a crucial requirement for successful transition prediction based on stability theory.

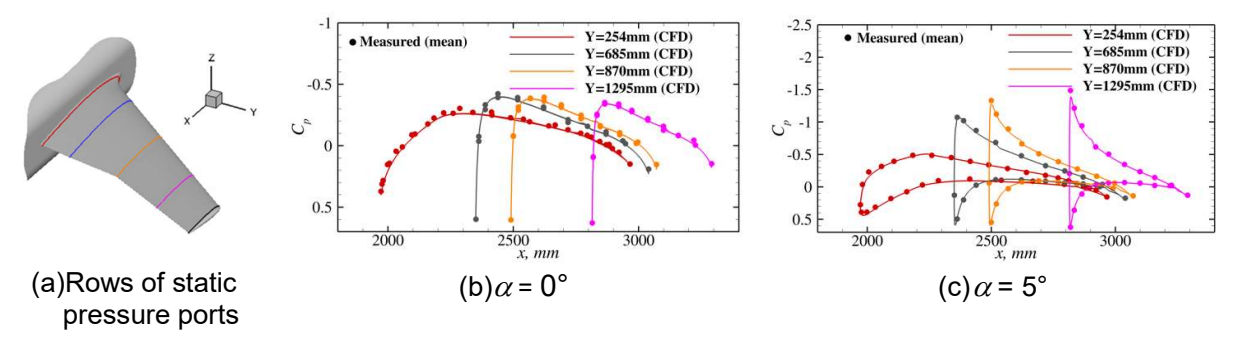


Figure 3 - Chordwise Cp distribution along static pressure rows on NASA Juncture Flow Model at M = 0.189, $Re_c = 2.4 \times 10^6$, and $T_{\infty} = 288.84$ K for two selected angles of attack. Color coding for the C_p plots is aligned with the spanwise cuts from part (a).

The change in upper surface pressure distribution from α = 0° to α = 5° illustrates two main effects: an advancing suction peak and an increasingly adverse pressure gradient downstream of this peak. Consistent with the adverse pressure gradient, the pre-test stability computations from [39] had shown that for α > 0°, the disturbance growth over the upper surface is dominated by the TS instabilities. The corresponding N-factor envelopes remained approximately parallel to the leading edge. A substantial reduction in the laminar flow extent was predicted from up to nearly mid-chord for α = 0° to only a short distance downstream of the attachment line for α = 7.5°. For negative angles of attack, an appreciable amplification of stationary crossflow (CF) instabilities was predicted over the upper surface from α = -4° to α = -7.5°, reducing the laminar flow extent within the inboard region of the wings.

Figure 4 (a) displays the predicted N-factors at various points along the measured transition fronts at $\alpha=0^\circ$ (blue symbols) and $\alpha=-4^\circ$ (magenta symbols). Based on the data for these two angles of attack, the parameters for the dual N-factor criterion were chosen as $N_{TS,c}=10$, $N_{CF,c}=6.2$, $a_{TS}=3$, and $a_{CF}=3$. The resulting front for $I(N_{TS},N_{CF})=1$ within the dual N-factor space is indicated in Fig. 4 (a).

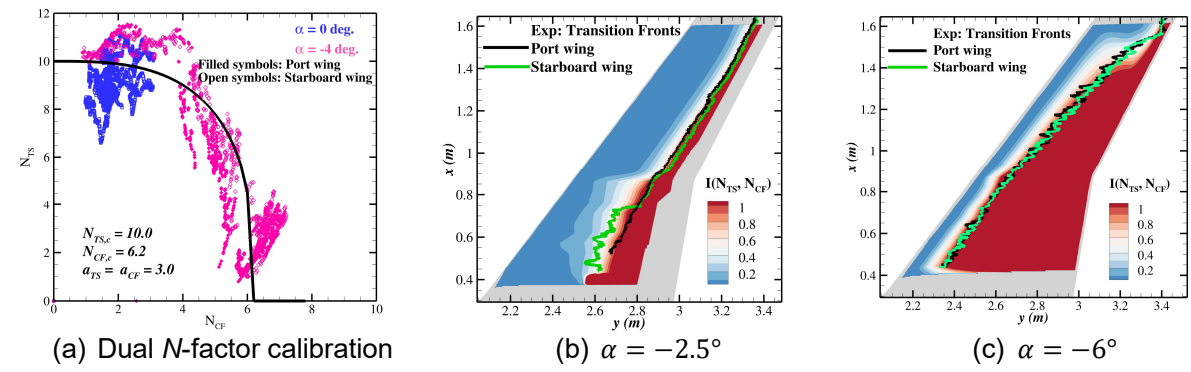


Figure 4 - Transition predictions based on a single iteration of the Stability-based approach for Juncture Flow Model at M = 0.189 and $Re_c = 2.4 \times 10^6$.

Figures 4(b) and 4(c) display contours of the indicator function $I(N_{TS},N_{CF})$ based on the above criterion for $\alpha=-2.5^{\circ}$ and $\alpha=-6^{\circ}$, respectively. The good overall agreement with the measured transition fronts indicates that satisfactory transition predictions can be obtained even when a small subset of the overall data from the same experiment is used to calibrate the dual N-factor criterion. While this demonstrates limited generalizability, it does not provide any clues regarding the accuracy of this calibration for other flow configurations within the same wind tunnel. In essence, such uncertainty is indicative of certain postdictive elements within such predictions. The relatively high value of $N_{TS,c}=10$ (larger than the estimate from Mack's correlation and measured Tu) is also intriguing and warrants further investigation. In principle, the predictive capabilities of the current set of stability-based transition models can be improved via more general criteria that incorporate the major sensitivities of the transition processes. However, this challenging endeavor will not be feasible without a major expansion of higher fidelity datasets (both experiments and simulations) that include a significant range of major parameters associated with the external disturbance environment.

3.2 Swept-wing configurations: NASA CRM-NLF Configuration

Application of natural laminar flow (NLF) to swept wing configurations on commercial transports offers a valuable test case for CFD-integrated transition models. This case is valuable due to its significance in aerospace applications and the technical challenges it presents, including the presence of shocks, accompanying viscous-inviscid interactions, and the coexistence of TS and CF instabilities. To extend and refine the iterative approach for stability-based transition modeling to 3D transonic wings, we have used the common research model with natural laminar flow (CRM-NLF) aircraft configuration [40]. Transition measurements for the CRM-NLF configuration had been obtained during wind tunnel tests in the National Transonic Facility at NASA Langley Research Center [41 – 43].

Computations by Paredes et al. [44] focused on the suction surface of the CRM-NLF wing, including four different angles of attack ($\alpha = 1.45^{\circ}$, 1.98°, 2.46°, and 2.94°) at a Reynolds number of $Re_{MAC} = 15 \times 10^6$, where MAC denotes the mean aerodynamic chord. Flow over the CRM-NLF wing includes a dual shock system and results presented below will show that the measured transition front is aligned with the shock front in the outboard region of the wing. For the cases of interest, TS amplification was always significant throughout the wing. Although stationary crossflow N-factors were smaller on certain parts of the wing, appreciable crossflow amplification was predicted in certain spanwise regions (in a narrow region around the break and in the outboard regions of the wing approaching the wing tip for $\alpha = 1.45^{\circ}$ and $\alpha = 1.98^{\circ}$). Therefore, similar to the Juncture Flow Model, transition over the CRM-NLF configuration was modeled with the dual N-factor method that accounts for both TS waves and the stationary CF instability. Results presented below are based on $N_{TS,c}$ = 6, $N_{CF,C}$ = 6, a_{TS} = 3, and a_{CF} = 3. The critical N-factor for TS waves was chosen on the basis of previous work by Crouch et al. [45]. The remaining two parameters from the dual N-factor criteria (namely, a_{TS} and a_{CF}) are related to the effects of interaction between the two modes of instability and were determined by trial and error [46]. Observe that the latter two parameters are identical for both the Juncture Flow Model and CRM-NLF experiments, despite significant differences between the two wind tunnels and the flow conditions of both experiments. This coincidence is encouraging, as it suggests that the calibration parameters associated with the TS-CF interaction do not vary greatly, at

least between these two cases. Earlier computations in Ref. [44] revealed that, with an imposed transition (IT) front along the measured locations on the suction surface of the CRM-NLF wing, the predicted shock locations on the suction surface were noticeably downstream of the shock locations from a fully turbulent solution. To ensure a consistent predictive procedure for the iterative transition analysis, the computations described here began with an initial transition front derived from the most upstream shock locations from a fully turbulent solution and iteratively updated the transition front using the predictions of the dual N-factor criterion.

Figure 5 illustrates the predicted transition fronts for $\alpha=1.45^\circ$ and $\alpha=1.98^\circ$ obtained with the dual N-factor method after three iterations of the coupled analysis, overlaid with TSP images and the inferred transition front from the experiment [43], along with the shock front predicted by the fully turbulent computations. The TSP images show a number of turbulent wedges emanating close to the leading edge. These wedges lead to uncertainty in the transition front, which may have contributed to the jaggedness of the transition fronts inferred from the TSP images. For both conditions shown in Fig. 5, the predicted transition front is upstream of the inferred front from the experiment in the region immediately inboard of the break, possibly because the TS and CF N-factors were comparable in this section. In general, the differences between the predicted and measured transition fronts are modest. The proximity of the transition front with the shock fronts from the underlying solution also underlines the coupling between the transition front and the shock system as mentioned earlier.

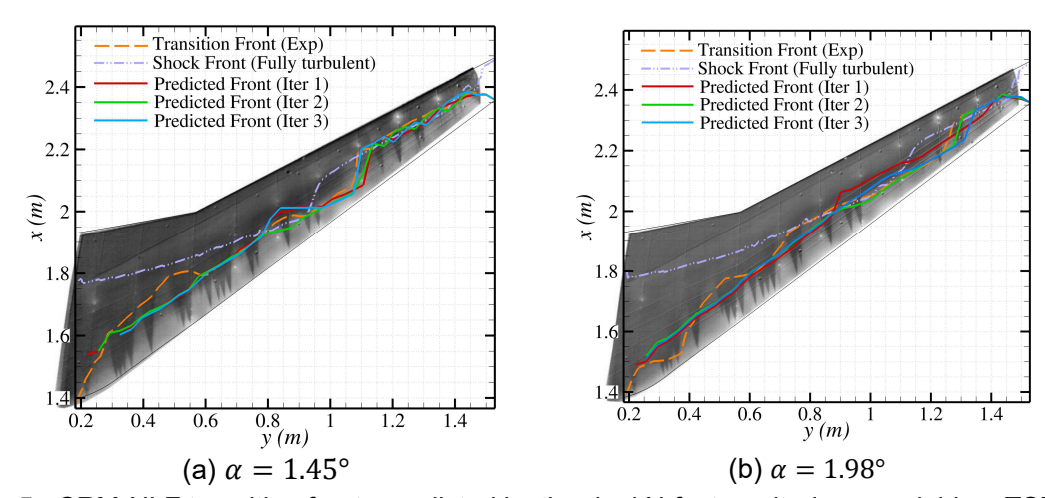


Figure 5 - CRM-NLF transition fronts predicted by the dual N-factor criterion, overlaid on TSP images obtained from the CRM-NLF experiment, along with the transition fronts inferred from those images [43] and the shock front from fully turbulent computations for two different angles of attack at M = 0.856 and $Re_{MAC} = 15 \times 10^6$.

Figure 6 shows the comparison of predicted surface pressure coefficients based on the transition model with the measured data along selected rows of pressure ports for $\alpha=1.45^\circ$. While the predicted pressure coefficients at the wingspan stations from the measurements (indicated by solid red curves) are fairly close to the measured values (marked by symbols), computations consistently indicate a downstream shift in the shock location compared to the experimental data. The measured shock locations agree better with the fully turbulent solutions (indicated by broken lines in blue). This shift highlights the sensitivity of the transonic wing flow to viscous-inviscid interaction effects, as well as revealing that the pressure ports likely tripped the experimental flow along those spanwise stations [42]. The latter may explain the better agreement of the measured values with the fully turbulent results.

There are still a few important lingering questions regarding the extraction of a transition front from the TSP images and the potential roles of both aeroelastic effects and surface roughness associated with tunnel particulates during the transition process over the CRM-NLF. However, irrespective of those issues, transition analysis for the CRM-NLF has been invaluable to our development of a CFD-integrated transition modeling framework. To our knowledge, this was also the first application demonstrating the feasibility of PSE-based integrated transition analysis for a transport wing.

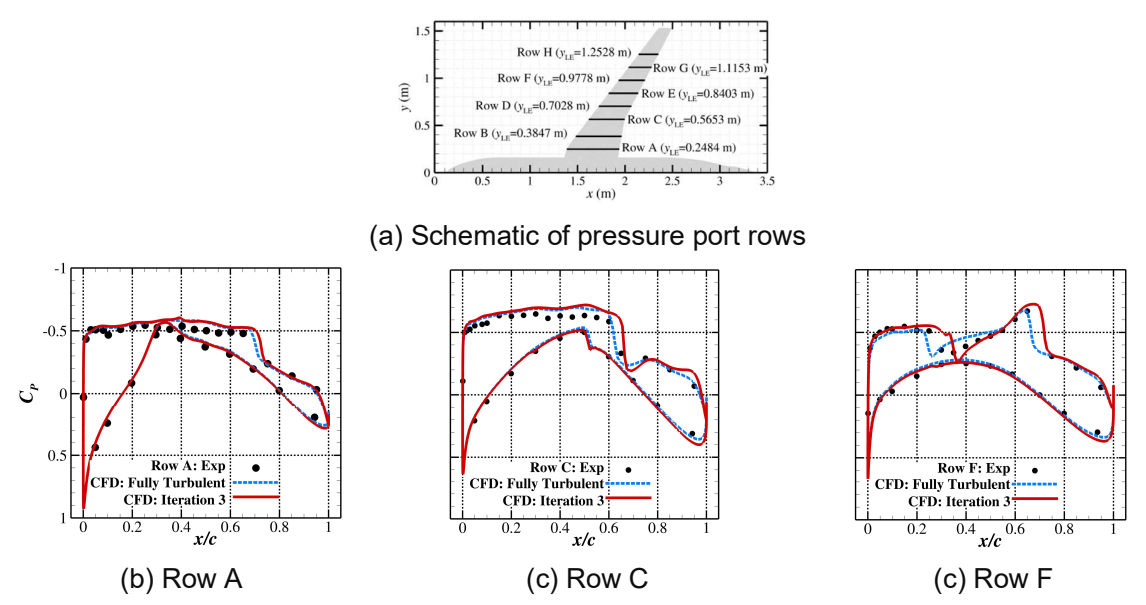


Figure 6 - Experimental and predicted C_p distributions at selected sections of CRM-NLF wing for 1.45° (M=0.856 and $Re_{MAC}=15\times10^6$).

3.3 High-Lift Configurations: 30P30N Multi-Element Airfoil Configuration

Flight experiments have revealed significant laminar flow regions on subsonic transport aircraft, even under "dirty" high-lift conditions with the leading-edge slat and trailing-edge flap(s) in a deployed setting [47]. These findings highlight the significance of transition modeling for high-lift predictions. Accurate prediction of transition to turbulence may also play a role in maximum-lift prediction, which is necessary for the certification of new commercial aircraft using CFD analysis methods.

The McDonnell Douglas 30P30N three-element airfoil is a well-known test case with high quality transition data for 2D high-lift configurations. It originated from the High-Lift Workshop/ CFD Challenge organized by the NASA Langley Research Center [48] and has also been used for the AIAA workshops related to airframe noise [49]. Transition over 3D high-lift configurations at flight-relevant Reynolds numbers may involve a plethora of transition mechanisms including attachment line transition, TS and crossflow instabilities, flow separation, wake-boundary layer interactions, and bypass transition due to surface imperfections. Additionally, relaminarization (and subsequent retransition) may occur due to the combined effects of pressure gradient, surface curvature, and Reynolds number. Furthermore, the convection of unsteady structures from one or more upstream regions of flow separation, combined with the acoustic noise generated via the interaction between those structures and the solid surfaces, can significantly modify the freestream disturbance environment encountered by the boundary layers.

Besides the aforementioned physical complexities, high-lift configurations also introduce implementation challenges for stability-based transition modeling. First of all, boundary layers develop on both sides of the different elements of the high-lift configuration and interact with the wakes from the upstream elements. Thus, the transition model implementation must isolate the various laminar portions of the viscous flow and then account for the differences in transition mechanisms associated with each portion. Additionally, when overset grids are used to simplify the grid generation process, accurate extraction of boundary layer profiles over the downstream elements involves extra challenges due to multiple overlapping grids. In that regard, a purely unstructured grid computation of the 30P30N configuration presents a simpler case with a limited subset of the above challenges, enabling comparisons with measurement data for a range of flow conditions.

As an illustration of the FUN3D capability, transition over the suction surface of the 30P30N slat at $\alpha = 8^{\circ}$ with M = 0.2 and a stowed-chord Reynolds number of $Re_c = 9$ million is considered here. Slat transition is important because of its relevance to the slat wake, which also interacts with the main

element and the flap, potentially impacting the overall aerodynamics. The selected flow condition has been extensively analyzed over the years, both for fully turbulent computations [50] and those including transition [51,52,11]. It also corresponds to one of the few conditions where transition does not involve a laminar separation bubble. Preliminary results for slat transition at the $\alpha=8^{\circ}$ condition are shown in Fig. 7. These computations were performed using a grid that was designed for RANS predictions rather than for stability computations. Nonetheless, they are sufficient to illustrate the feasibility of performing automated PSE-based stability analysis for multi-element airfoils using the LASTRAC-FUN3D integration. More detailed transition analysis for the 30P30N configuration is currently under way and the results of that analysis will be described in an upcoming paper [53].

The predicted transition onset location over the slat is marked in Fig. 7(a) with an open triangle; the slat contour is colored by the N-factor values and N-factors of 7, 8, 9, and 10 are marked with parallel lines interacting the slat contour at the corresponding surface locations. The N-factor correlation of N_{tr} = 9 was chosen on the basis of the earlier work by Malik and Lin [51], which also used PSE-based transition prediction. The flight-like N-factor is also consistent with the low levels of freestream turbulence in the Low Turbulence Pressure Tunnel (LTPT). The computational result in Fig. 7(a) indicates a significantly delayed onset of transition relative to the reported measurement of transition onset location (indicated by the upstream hollow circle on the plot). However, a scrutiny of the overall body of measured transition data [54] reveals that the measured locations of the start and end of slat transition at this particular condition are outliers relative to the remaining data. When the transition onset location at the condition of interest is interpolated from the neighboring conditions, a monotonic variation with respect to the flow parameters is found. The predicted transition location indicates improved agreement with the interpolated transition onset location, which is indicated by a star in Fig. 7(a) that overlaps with the open triangle.

Thus, at least for the $\alpha=8^\circ$ case, the stability model seems to provide reasonable prediction of transition over the slat suction surface at the relatively low freestream turbulence intensity of less than 0.1%. In contrast, previously published work [52] using the phenomenological LM2009 model was not able to capture the slat transition behavior at this angle of attack until the freestream turbulence was increased to 0.8%. Although not shown in Fig. 7, the FUN3D transition model is capable of applying stability-based transition prediction to multiple elements of the high-lift configuration including the main wing and the flap. For instance, rather low values of N-factor were predicted along the lower flap surface, which is consistent with the laminar behavior inferred from the experimental measurements [55].

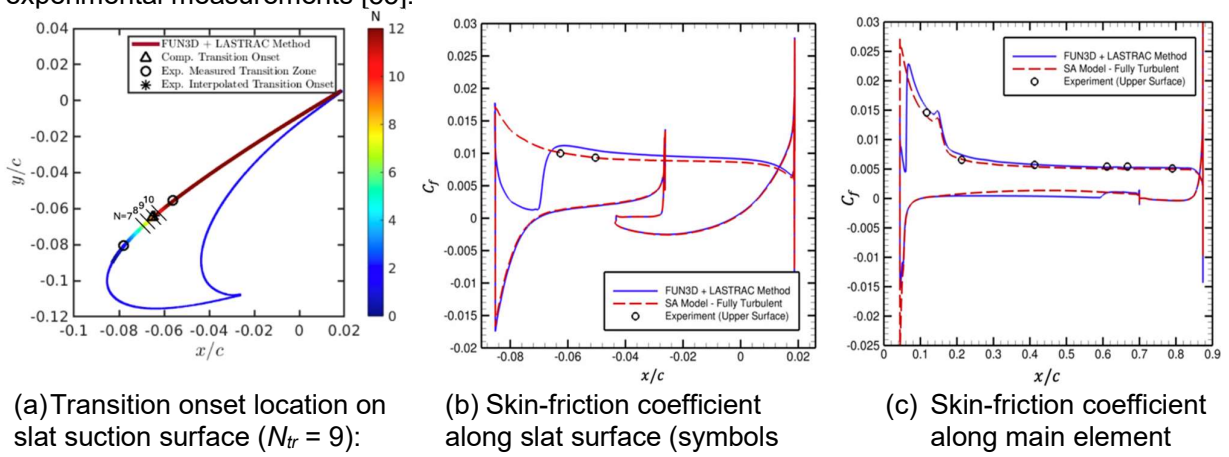


Figure 7 - Stability-based transition predictions for 30P30N multi-element airfoil at M = 0.2, $\alpha = 8^{\circ}$, and $Re_c = 9 \times 10^6$.

indicate measured data)

3.4 Hypersonic Flows

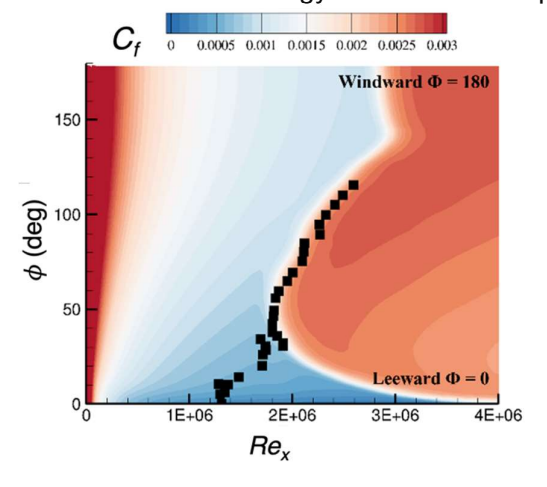
comparison with experiment

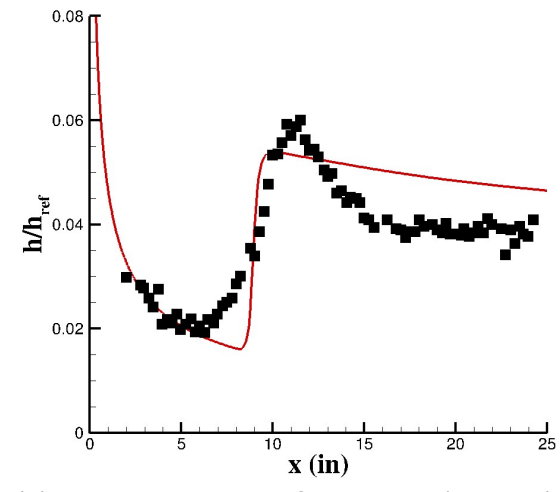
The prediction of laminar-turbulent transition in high-speed flows is critical to designing flight systems because of its importance in determining the heat load. However, this prediction faces challenges due to compressible flow phenomena, combined with an increased variety of transition mechanisms. Despite these challenges, advancement of transition modeling for high-speed flows remains an essential need as described by the CFD 2030 Vision study [1]. To address that need, NASA Langley Research Center has undertaken research to integrate stability-based transition models for high-

speed flows with CFD solvers and to enhance the maturity of transport-equations-based transition models that can be applied in high-speed flows. Recent progress in stability-based modeling is summarized in this section.

Illustrative results for transition in canonical supersonic and hypersonic flows are shown in Fig. 8. Here, the line and surface plots represent the predictions of the coupled transition analysis, while the solid squares represent the experimental data from Refs. [56] and [57] for subfigures 8(a) and 8(b), respectively. The initial implementation of coupled stability analysis for supersonic and hypersonic flows is described in Ref. [58]. However, the transition N-factor estimation and intermittency prescription described in that work have since been superseded by further enhancements as outlined below.

Stability-based transition prediction requires the user to specify the transition N-factor, N_{tr} , which varies considerably across high-speed applications depending on the dominant instability mechanism and the relevant disturbance environment. This uncertainty underscores the need for more general criteria based on easily input parameters, which would reduce the post-dictive element of the N-factor methodology and enhance its predictive capabilities.





- (a) Skin friction coefficient predicted after 3 iterations of CFD-LASTRAC analysis for 5-degree half angle cone at Mach 2, 2° angle-of-attack, N_{tr} = 7 (symbols denote measured data from Tokugawa et al. [57])
- (b) Axial distribution of predicted (red line) and measured (symbols) nondimensional heat transfer coefficient for 5-degree half angle cone with blunted tip at Mach 6, 0° angle-of-attack, N_{tr} = 5.5 (experiment by Horvath et al.[56])

Figure 8 - Illustration of coupled OVERFLOW-LASTRAC analysis for two straight-cone configurations in supersonic and hypersonic flows, respectively. Figures reproduced from [58].

To provide an engineering solution for determining N_{tr} for experiments in conventional hypersonic wind tunnels, Vogel and Choudhari [59] developed a correlation based on 45 hypersonic ground test cases of canonical geometries. This correlation expands the existing correlations for straight circular cones with a narrow range of half angles to a broader array of second-mode-dominant axisymmetric configurations without requiring an extensive amount of configuration-specific data. The input arguments for this correlation include easily available quantities such as the freestream disturbance intensity, Mach number, and body-based slenderness Reynolds number.

The details of the above correlation can be found in [59]; however, its two main components correspond to the disturbance amplitude at the onset of transition (related to the saturation amplitude A_{max} for Mack's second mode instabilities) and the receptivity coefficient C_R that relates the initial instability amplitude to freestream disturbance intensity. Figures 9(a) and 9(b) compare the correlated values of these parameters with those estimated for the experimental configurations used as the training data. Figure 9(c) displays the comparison between the N-factors computed at the measured transition locations and those predicted by this correlation. Future work will focus on a more in-depth evaluation of this correlation and on enhancing its generalizability.

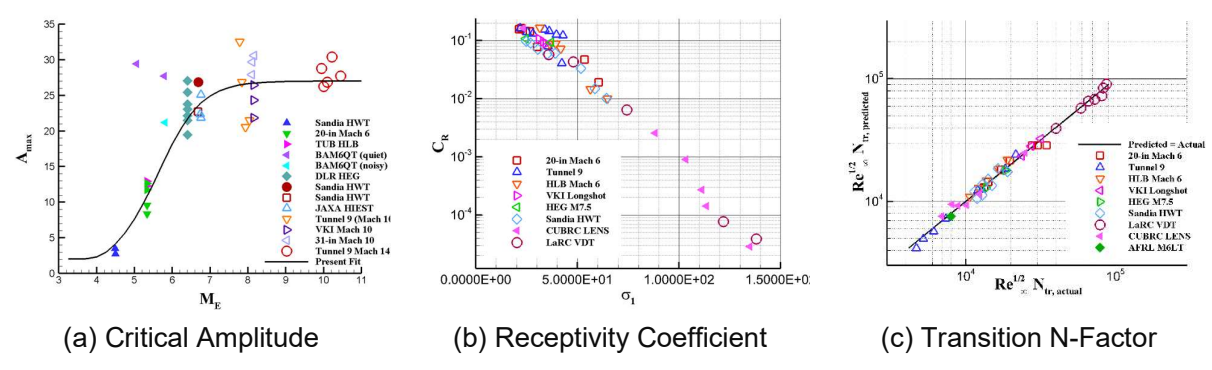


Figure 9 - Illustration of the curve fits from [59] for two main components of the empirical correlation involving the transition N-factor (N_{tr}) related to 2^{nd} mode dominated transition in conventional ground test tunnels. Symbols indicate the values of each component correlation based on the training cases. Part (c) indicates the overall accuracy of the correlation.

The locations of transition onset correspond to the dominant source of transition-related uncertainty in predicting the aerothermodynamic environment of hypersonic vehicles. However, the extent of the transition zone can also impact the total heat load, especially when the transition zone has a significant extent. The peak local heat transfer is also a crucial metric that depends on the details of the transition zone and the potential overshoot in heat transfer distribution. To help address the need for transition zone modeling, current work is focused on developing a correlation for the intermittency distribution that will be coupled with the SA turbulence model. Figure 10 presents preliminary predictions of the forthcoming correlation and compares them with the measured data and also with a baseline intermittency model from [58]. We note that neither of the cases shown in this figure were used in the development of the correlation. Although this figure represents ongoing work, the present correlation shows encouraging agreement with the experimental heat transfer coefficients in spite of being derived from a small pool of training cases. Further results based on this intermittency model will be presented in a forthcoming paper.

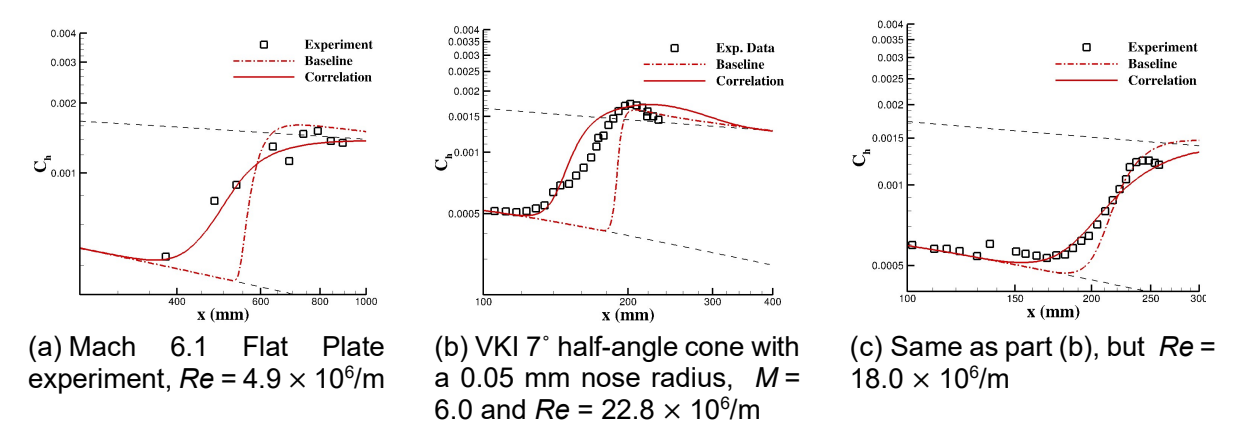


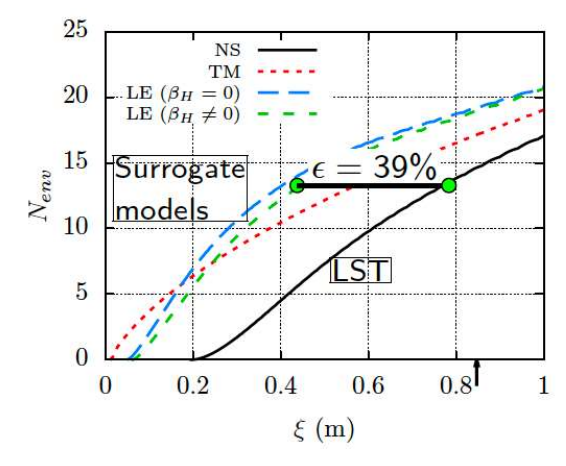
Figure 10 - Demonstration of the intermittency correlation for CFD-stability coupled transition prediction. Curves labeled "Baseline" denote the predictions of a simple model used in earlier results [58] whereas the curves labeled "Correlation" utilize the preliminary correlation mentioned in the text. Experimental data is indicated by symbols.

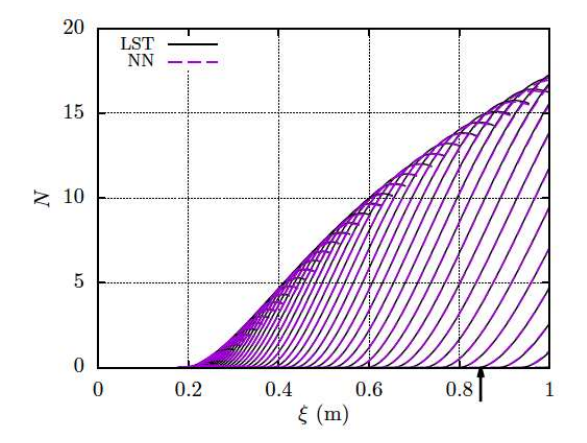
3.5 Surrogate Stability Models Based on Deep Learning

Traditional surrogates for linear-stability based transition models are derived from existing databases of precomputed stability characteristics. The surrogates create an analytical or numerical response surface model in terms of a small number of scalar input parameters that represent a combination of global flow parameters, selected attributes of boundary layer profiles, and relevant disturbance characteristics such as frequency and wave-number parameters. However, these traditional methods face limitations when applied to flow configurations where the transition process depends on a large set of factors such as surface temperature, suction/blowing, roughness, edge Mach number, non-equilibrium phenomena in high enthalpy flows, etc.

In contrast, neural network methods are able to accommodate higher dimensional input features to be considered without compromising the efficiency and accuracy compared to the traditional data driven models. This capability allows for more comprehensive analysis of complex flow configurations. However, neural network-based surrogate models often face challenges related to generalizability and interpretability. To investigate the potential of neural networks in transition prediction and help address the associated challenges, we have experimented with several architectures, including convolutional neural networks (CNN) [32], recurrent neural networks (RNN) [31], and simpler fully connected networks (FCN) [30]. The CNN and RNN models integrated a convolutional encoder with an FCN-based predictor of the local slope of an N-factor curve. The dominant latent feature identified by the encoder strongly correlated with the shape factor of the local velocity profile, providing some interpretability to the CNN model [32]. While both the CNN and the FCN architectures modeled the N-factor curve for a single disturbance entity (i.e., a fixed combination of frequency and spanwise wavenumber), the RNN focused on directly modeling the N-factor envelope for a given flow. In recent work, we have used the proper orthogonal decomposition coefficients of the velocity profiles to reduce the input space dimensionality for FCN models and obtained similar results as the earlier CNN model [32].

Figure 11 taken from [33] demonstrates the application of the CNN model to second mode amplification on a 7-degree half-angle cone with 2.5 mm nose radius during ascent phase of the HiFIRE-1 flight experiment [60]. The results compare the direct stability computations using Linear Stability Theory (LST) with two surrogate models: (i) A model trained on self-similar, sharp-cone boundary layer profiles (a common approach in surrogate model development) with edge values and boundary-layer thickness as correlating parameters, both with and without local pressure gradient effects, and (ii) a CNN model based on Navier-Stokes basic state solutions for a 7-degree half-angle cone with 2.5 mm nose radius and various freestream conditions and surface temperature ratios. The growth rate predictions based on the equivalent self-similar profiles were consistently larger than for those calculated with the Navier-Stokes basic state, resulting in approximately 39% underprediction of the transition onset location. This discrepancy is attributed to the modified boundary layer profiles due to entropy layer effects, which are not adequately captured by the local boundary-layer edge properties and thickness.





- (a) Comparison of N-factor envelopes predicted by LST for various mean-flow approximations: Navier-Stokes (NS), locally self-similar profiles based on Taylor-Maccoll (TM) post-shock conditions and self-similar approximations based on local edge conditions (LE) with zero or nonzero Hartree pressure gradient parameter β_H .
- (b) Comparison of N-factor curves for constant frequency instability modes predicted by LST and its (convolutional) neural network (NN) surrogate. The vertical arrow indicates the measured transition location.

Figure 11 - Application of surrogate models to predict amplification characteristics of axisymmetric Mack-mode disturbances over the HIFiRE-1 flight vehicle at a flight ascent time of t = 21.5 sec.

Figure 11(b) demonstrates the accuracy of the CNN predictions, indicating excellent agreement with the LST data. The CNN model also exhibited moderate generalizability beyond its

degree angle of attack, $Re_c = 9 \times 10^6$

training data, successfully predicting second mode amplification for test cases involving cones with nonuniform surface temperature distributions, a 5-degree cone despite being trained on 7-degree cases, and even freestream conditions that amounted to an extrapolation beyond the training space. Additionally, it showed some robustness to under-resolved basic states. However, further generalization of the model to a broader range of flow configurations remains to be investigated.

An important means of enhancing the generalizability of a neural network model is to increase the breadth of the training data. To that end, a large database comprised of the linear growth characteristics of over 35,000 boundary-layer flows over 56 airfoils at varying Reynolds numbers and angles of attack has been used to enable the training and testing of surrogate models for transition due to TS instabilities. Computationally, it's much more expedient to use a boundary-layer code to generate the mean boundary layer profiles for generating a large database of this type. On the other hand, the target application space for CFD integrated transition modeling involves mean profiles extracted from Navier-Stokes solutions, which do not asymptote to a uniform behavior beyond the boundary layer edge (Fig. 12(a)). Thus, in order to apply the surrogate model to CFD-integrated transition prediction, it is essential to determine how to align the two classes of profiles. Our approach to this challenge has been to transform the N-S profiles into profiles that asymptotically approach uniform behavior in the freestream, analogous to those obtained via boundary-layer codes. This mapping was accomplished using a physical interpretation of the boundary-layer integral thickness parameters. This mapping enables one to easily determine the edge of the boundary layer, and hence, to estimate the flow quantities at the edge of the boundary layer and the integral parameters of the boundary layer profiles (displacement thickness δ^* , momentum thickness θ and shape factor H). A seamless integration of the neural net models into the framework from Fig. 2 could be accomplished via Python utilities with the same input-output interface as the LASTRAC stability code.

Figure 12(b) illustrates the application of the neural network model for TS instabilities to natural transition in a fully attached boundary layer over a NLF-0416 Airfoil at 0-degree angle of attack, and chord Reynolds number of $Re_c = 9 \times 10^6$, indicating the good agreement with the LST data across a broad range of frequencies.

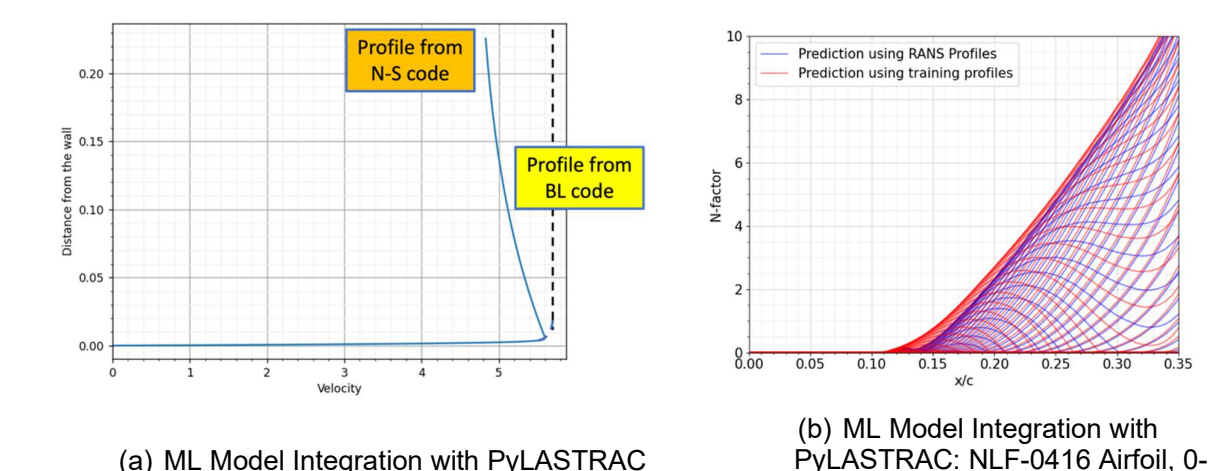


Figure 12 - Neural network model for TS wave amplification in low-speed boundary layers

In summary, neural network based surrogate models for stability characteristics offer a promising alternative to direct stability computations. These models are more robust and user-friendly, making them well suited for CFD users who may not have extensive expertise in stability theory. Coupled with the models' capability to generate satisfactory transition predictions with high efficiency, they could be leveraged during the conceptual design phase as a useful means of conducting trajectory assessments. In addition to the surrogate models for stability, an ongoing model augmentation effort aims to use data-driven techniques based on field inversion and machine learning to improve the predictions for the transport-equations-based transition models such as the Langtry-Menter [9] and AFT [15] models using available higher-fidelity data for flows where compressibility and/or surface roughness can significantly influence the transition locations.

3.6 Design Optimization

As described in Section 1, the development of CFD integrated transition modeling methodologies is crucial for the development of future aircraft with substantially reduced environmental impact. NASA's aeronautics plan and ICAO aim to reduce the aviation CO₂ emissions by 50% (relative to 2005 levels) by 2050. Aircraft drag reduction via both natural laminar flow (NLF) and hybrid laminar flow control (HLFC), which combines NLF with suction near the leading edge, offers considerable potential for improved aircraft efficiency and reduced emissions of greenhouse gases. The N+3 and N+4 concepts for future aircraft proposed under NASA sponsored research rely on NLF to achieve the drag reduction benefit provided by laminar flow, but any uncertainties in transition modeling can significantly offset the projected benefits of NLF. Our ongoing effort as described in Section 2 has targeted improved transition models that should help reduce these uncertainties. Yet, developing better transition models alone is not sufficient. To fully realize the potential of laminar flow technology, the enhanced transition modeling capability must also be integrated into aerodynamic design tools that would enable engineers to create designs that can achieve the projected benefits of NLF and HLFC in practice.

In recent years, knowledge-based NLF design practices have been successfully used to develop novel swept-wing configurations that may provide significant reductions in overall drag [61]. Adjoint-based design approaches offer a complementary approach with several attractive features. Specifically, it provides scalability to a large number of design variables, comprehensive sensitivity information, ability to satisfy multiple objectives/constraints including off-design performance, and amenability to automation and fast design iterations. A number of prior studies have presented adjoint-based NLF design using transport equations for transition prediction (e.g., Ref. [62]) and data-driven surrogates [63,64] to stability models. However, the CFD integration of transition models that utilize direct stability computations opens up the possibility of using higher-fidelity transition prediction within the adjoint-based design framework. Design capability based on the direct computation of stability characteristics as described in the earlier sections has recently been implemented in NASA's FUN3D flow solver. Figure 13 depicts a schematic of this algorithm and the reader is deferred to a forthcoming paper [65] for additional details.

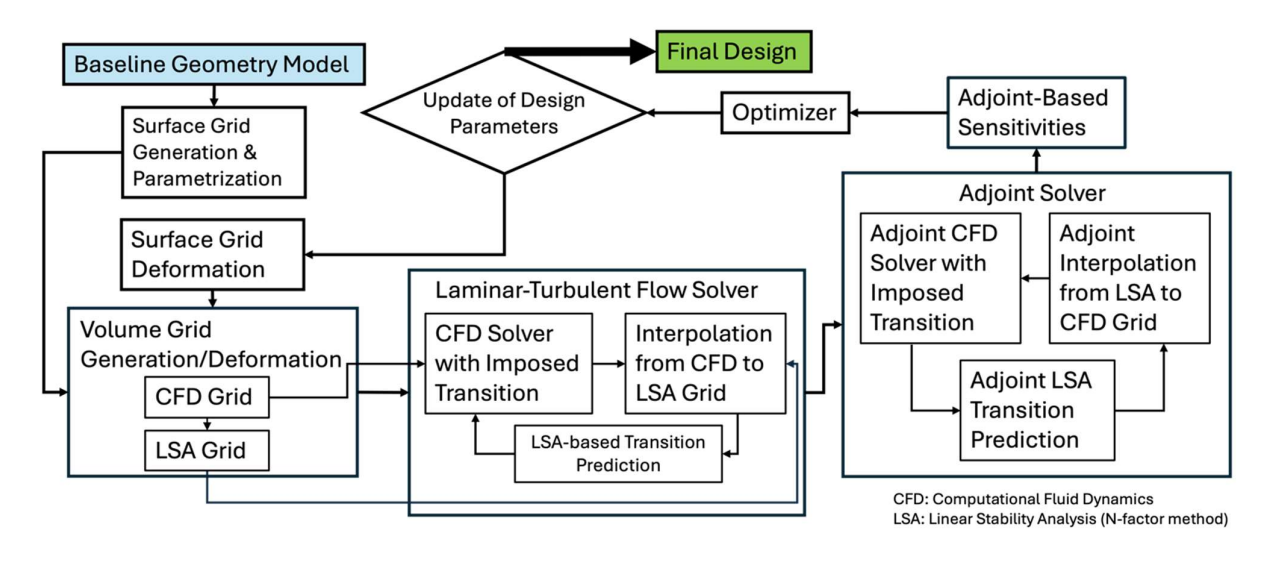


Figure 13 - Computational framework for stability-based design optimization. Figure reproduced from [65]. LSA denotes linear stability analysis.

4. Transport-Equations-based Transition Models

4.1 Low Reynolds Number Flows with 3D Separation Bubbles: Pazy Wing Configuration

The Pazy wing from the AIAA 3^{rd} Aeroelastic Prediction Workshop [66] is a highly flexible wing designed to study large deformations and nonlinear phenomena at low Reynolds numbers (Re_c =

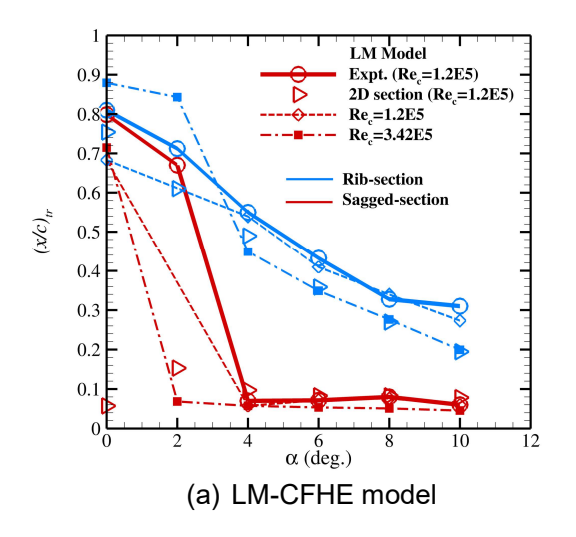
 1.2×10^5). The unique structural design of this wing features a spanwise array of thirteen ribs that leads to quasi-periodic sagging between the ribs. This sagging results in a spanwise varying sectional geometry that provides an interesting case for investigating the performance of transport-equations-based transition models.

Venkatachari et al. [67] reported steady-state computations of the Pazy wing at two different chord Reynolds numbers ($Re_c = 1.2 \times 10^5$ and $Re_c = 3.42 \times 10^5$) and several angles of attack. Different variants of the Langtry-Menter transition model, both with and without crossflow effects, were applied to the sagged Pazy wing. Results indicated that crossflow is unimportant for this configuration and that the primary transition mechanism is related to the presence of laminar separation bubbles (LSBs). Thus, additional computations were performed for 2D airfoils with cross sections representing the rib section and the center plane of the sagging regions, respectively. The rib section was modeled as the NACA-0018 airfoil, since it forms the basis for the unsagged Pazy wing and also has additional data available in the literature [68]. Ref. [67] compared their predictions for the Pazy wing based on two-equation transition models with those of Ritter et al. [69], who used the single-equation γ transition model from DLR. To align with [69], computations in [67] used Tu = 0.3%, slightly below the reported value of Tu = 0.5% in the wind tunnel. Despite this difference, comparisons with the wind tunnel measurements should offer useful insights into the transition model behavior of the Pazy wing. Nonetheless, the influence of this discrepancy should be considered when interpreting the following results that were obtained via the helicity-based crossflow extension [17] to the LM2009 model (denoted here as the LM-CFHE model) and the AFT2017b Model [70] (henceforth referred to as simply the AFT model).

The transition location in 2D LSBs correlates with the end of the plateau in the chordwise Cp distribution near the LSB [68, 71]. Given the minimal effects of crossflow as mentioned before, the observed correlation from Refs. [68, 71] was used to estimate the computational transition locations along the rib section and the sagged sections of the wing. A comparison of the IR-based experimental transition locations [72] with the predictions of the LM-CFHE is shown in Fig.14(a), whereas similar results for the AFT model are plotted in Fig. 14(b). Transition predictions for the 2D sections at Re_c = 1.2×10^5 are also included for comparison. At $\alpha = 0^\circ$ and $\alpha = 2^\circ$, the observed transition is aft of x/c = 0.65 in both rib (solid blue curve) and sagged regions (solid red curve), with similar transition locations within those regions. For $\alpha = 0^{\circ}$, the measured transition location is bracketed by the LM-CFHE predictions at $Re_c = 1.2 \times 10^5$ (dashed curves in Fig.14) and $Re_c = 3.42 \times 10^5$ (dash-dot curves). At higher angles of attack, both measured and predicted transition locations along the rib indicate a smooth upstream trend. In contrast, measurements in the sagged region reveal an abrupt upstream shift to x/c < 0.1 when α is increased from 2° to 4°, and the transition location remains relatively unchanged for $\alpha > 4^{\circ}$. In comparison, 2D computations for the sagged section at Re_c = 1.2×10^5 (indicated by right-facing triangles in Fig.14) predict transition closer to the leading edge for all angles of attack studied here, i.e., including the $\alpha = 0^{\circ}$ and $\alpha = 2^{\circ}$ cases.

It may be observed that both LM-CFHE and AFT models capture the shift to upstream transition locations for $\alpha > 4^\circ$ and, in fact, agree rather well with the measured data. At these angles, the corresponding predictions at $Re_c = 3.42 \times 10^5$ are noticeably more upstream than the transition locations at $Re_c = 1.2 \times 10^5$. Computed results at $\alpha = 2^\circ$ for $Re_c = 1.2 \times 10^5$ are not yet available but would provide a more thorough assessment of the models. An examination of skin friction contours over the suction surface provides further insight into the above trends as described below.

Skin friction contours for $\alpha=0^\circ$ are presented in Fig. 15(a). Figure 15(b) shows analogous results for $\alpha=6^\circ$, which will be discussed later. For $Re_c=3.42\times10^5$, the $\alpha=0^\circ$ solutions based on the LM-CFHE model (as well as the AFT results not shown here) indicate a short separation bubble just downstream of the wing leading edge within the sagged regions along the span. The term separation is used broadly in this 3D context, to denote the onset of flow reversal along the chordwise direction. The bubbles appear as light colored regions in the figure and are marked by black lines. The bubbles reattach without any transition as observed from Fig. 14(a). At $Re_c=1.2\times10^5$, only a small number of sagged sections include the leading-edge LSBs in the LM-CFHE solution, indicating that the Pazy wing flow at $\alpha=0^\circ$ may be on the threshold of separation inside the sagged portions of the leading-edge region. The IR images from the wind tunnel experiment (not shown here) do not present any evidence of leading edge LSBs. These findings partially corroborate the LM-CFHE predictions at the lower Re_c , and the minor discrepancy in the computed results could be related to the lower value of Tu used in the computations.



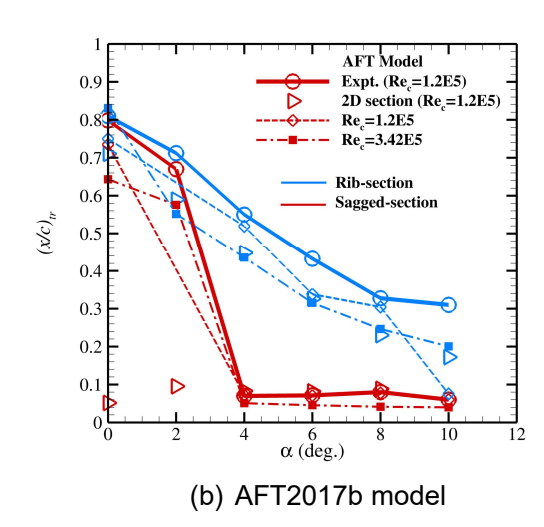


Figure 14 - Comparison of predicted and measured transition locations along the rib section (blue lines and symbols) and centerplane of the sagged section (red lines and symbols) for several angles of attack. Results are obtained by including sustaining terms for freestream turbulence.

At both Reynolds numbers, computed solutions at $\alpha=0^\circ$ display an additional region of separation that begins aft of the mid-chord location and extends across the entire span of the wing. At the lower Re_c , the LM-CFHE solution indicates a closed separation bubble with nearly uniform separation and reattachment fronts along the span. The corresponding AFT solution predicts delayed onset of separation in the vicinity of the rib section, resulting in prominent spanwise variations in the separation front. Additionally, the downstream bubble in the AFT solution remains open over most of the span. As the Reynolds number increases to $Re_c=3.42\times10^5$, the bubble from the LM-CFHE solution also exhibits spanwise variations along the separation and reattachment boundaries, along with a downstream shift near the rib section. Furthermore, the onset of separation moves downstream with respect to the lower Reynolds number case and the chordwise length of the bubble is reduced.

Figure 15(b) illustrates the flow behavior over the suction surface at α = 6°. The α = 6° solutions in Fig. 15(b) are representative of the higher angles of attack (α > 4°) until stall is reached. The α = 4° condition is more nuanced and will be discussed in detail in a forthcoming paper. The computed solutions in this range reveal two distinct changes with respect to the α = 0° case. First, all three computational solutions in Fig. 15(b) indicate the leading-edge separation bubbles inside the sagged regions. As discussed in the context of Fig. 14, the more robust LSBs under these conditions induce transition prior to their reattachment, which accounts for the abrupt upstream shift in the measured transition. The stronger adverse pressure gradient over the suction surface also leads to an additional LSB centered on the rib section. The extent of the rib LSB is upstream in comparison with the α = 0° case and the planform shape of this LSB includes narrow tails along its lateral boundaries that extend significantly downstream. Indeed, for the AFT model, the tails of the rib LSB even connect with the spanwise varying separation pockets in the trailing edge region.

In summary, the Pazy wing transition analysis has extended the assessment of mainstream transition models by evaluating their predictive capabilities for a spanwise quasi-periodic configuration that exhibits an intricate pattern of 3D separation bubbles. Related findings from [67] have also shown a strong code-to-code comparison with FUN3D predictions obtained using more modest grid resolutions that are typical of more complex geometries encountered in practice. That comparison has paved the way for applying the FUN3D transition models to more complex applications with aeroelastic phenomena.

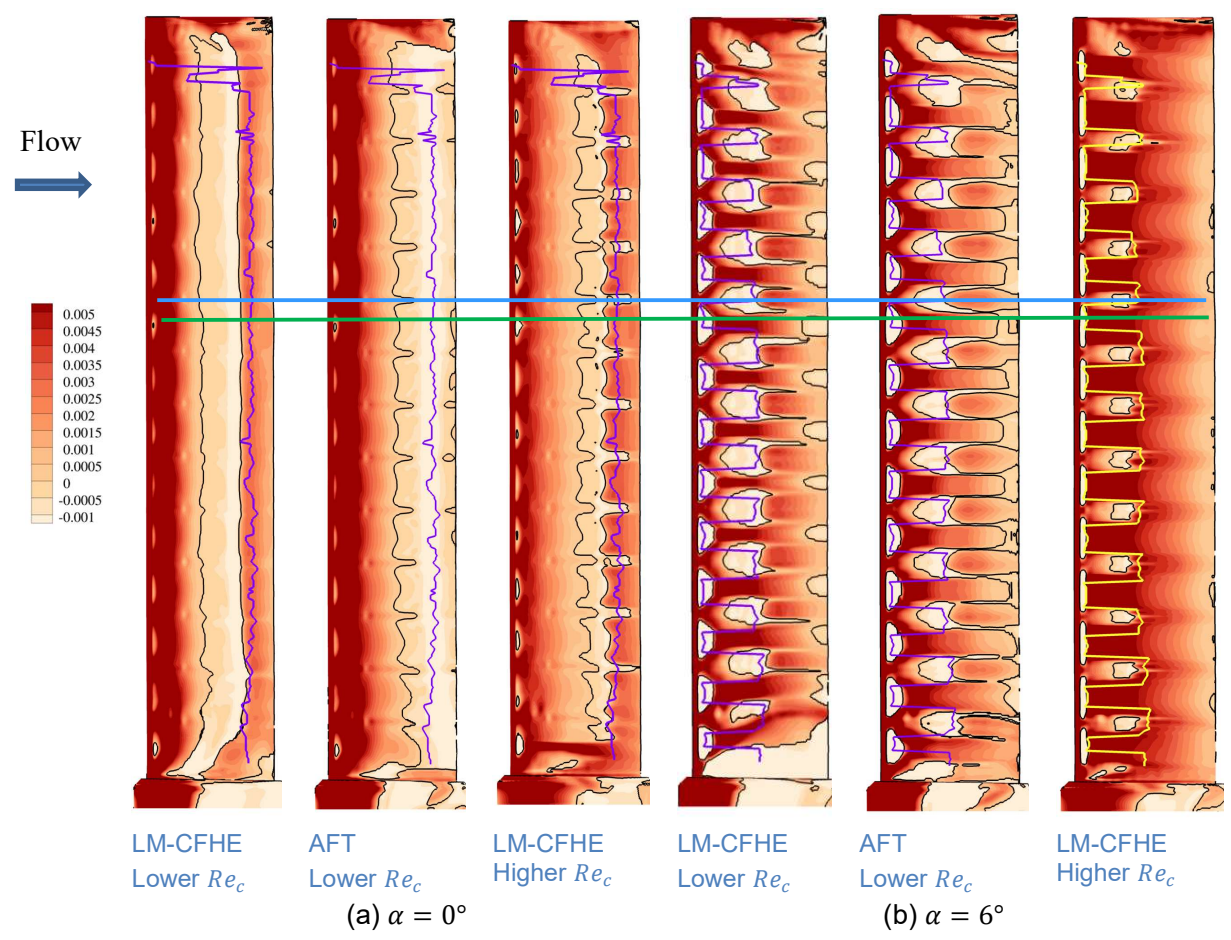


Figure 15 - Contours of skin friction coefficient C_f on the upper surface of sagged Pazy wing. Results are shown for both transition models at the lower $Re_c = 1.20 \times 10^5$ and only for the LM-CFHE model at the higher $Re_c = 3.42 \times 10^5$. Flow direction is from left to right. Experimentally inferred transition fronts [72] at $Re_c = 1.20 \times 10^5$ are shown as purple lines (yellow in rightmost plot for improved contrast to the underlying C_f contours). Black lines mark the locus of surface locations where the chordwise component of the skin-friction vector becomes zero. The blue and green horizontal lines indicate the rib- and sagged sections, respectively, corresponding to the 2D data in the previous figure.

4.2 Swept-wing configurations: NASA Juncture Flow Model

The Juncture Flow Model from Section 3.1 was also used to evaluate the predictions of three different variants of the LM transition model at flow conditions with significant potential interaction between TS and CF instabilities ($\alpha = -6^{\circ}$). As the LM2009 model does not include any CF effects, its predictions did not match the measured trends in transition (Fig. 16(a)). Despite the neglect of roughness effects that significantly influence the transition process at low levels of freestream unsteadiness, the predictions of the local-helicity-based LM-CFHE model (Fig.16(b)) were consistently in close agreement with the experimentally visualized transition front. In contrast, the roughness-sensitized LM2015 model predicted larger than measured laminar extent at the conditions examined during computations (Fig. 16(c)). Partial explanations for this discrepancy may be that (i) the limited measurements of surface roughness were not adequately representative of the roughness distribution across the entire span and/or that (ii) the effects of surface roughness cannot be captured by a single parameter in the form of the root-mean-square (rms) height, R_{α} . However, computations not shown here also indicated that the predicted transition front did not shift sufficiently upstream even when the input value of R_a was increased through a large range. Since crossflow effects were clearly significant in this case, the latter finding could be an indication that the original calibration of the LM2015 CF model [16], which was based on a rather sparse database, does not generalize well to the Juncture Flow Model experiment.

The experimental data also included transition measurements over the fuselage of the Juncture Flow Model and the LM-CFHE model was again able to match the azimuthal variations in the measured

transition front rather well, in addition to its excellent performance in predicting transition over both sides of the wing surface as seen from Fig. 17 for $\alpha = -7.5^{\circ}$.

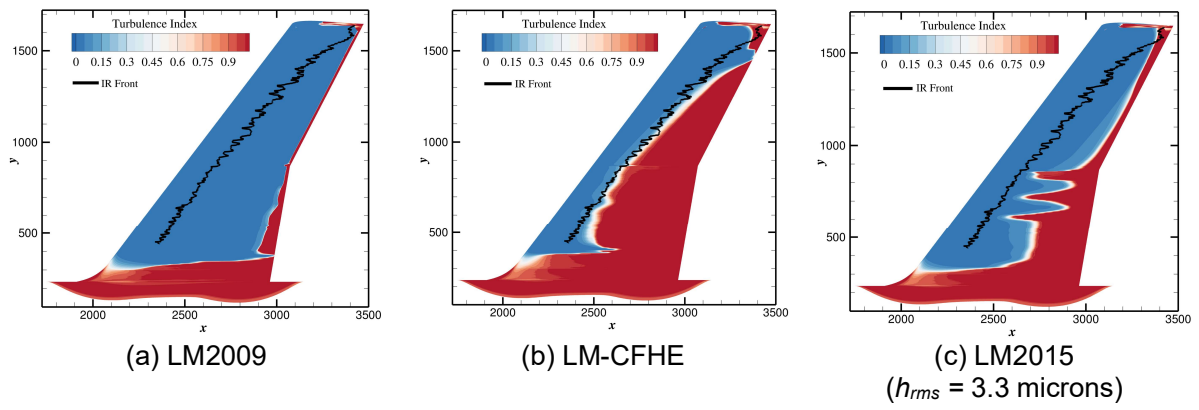


Figure 16 - Predicted transition behavior as depicted via turbulence index contours for $\alpha = -6^{\circ}$ obtained using different transition models. Black lines indicate transition fronts inferred from measurements. The red contours are indicative of fully turbulent flow in the computed solution.

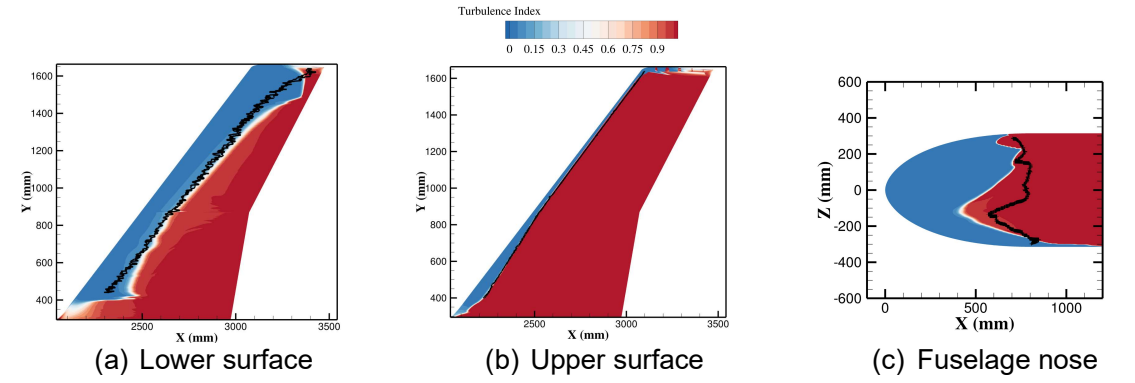


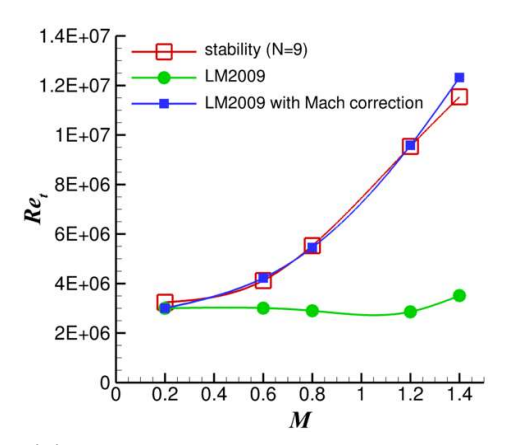
Figure 17 - Predicted transition behavior as depicted via turbulence index contours for $\alpha = -7.5^{\circ}$ obtained with the LM-CFHE model. Black lines indicate transition fronts inferred from measurements.

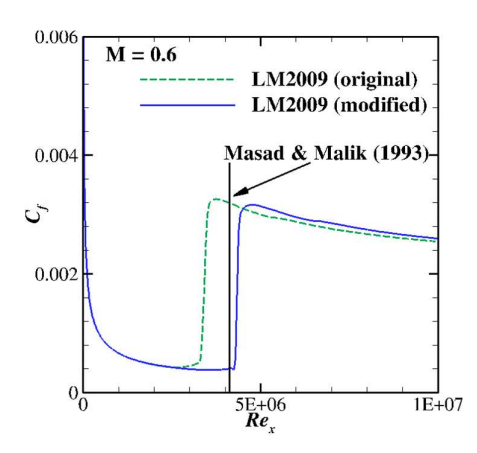
4.3 Compressibility Effects at Transonic Speeds

The LM model [111] is one of the most widely used models for predicting transition in RANS solvers. However, it relies on empirical correlations based on low-speed flows and does not account for the stabilizing influence of compressibility on the amplification of boundary layer instabilities [73]. As shown by Venkatachari et al. [74], this leads to significant underprediction of the laminar flow extent on two different wind tunnel configurations of particular significance: the NASA Common Research Model (CRM) and the CRM with Natural Laminar Flow (CRM-NLF) [40-43]. Based on those findings, a systematic evaluation of the predictive accuracy of the LM transition model for transonic boundary layers in low disturbance environments was performed. Results showed that the accuracy of the LM model was impacted mainly for near-zero to favorable pressure gradients, an important class of flows that is relevant to natural laminar flow wings. To address this issue, a straightforward modification was proposed to incorporate compressibility effects into the LM model. Correction factors based on the local value of edge Mach number modified a subset of relevant correlations from the LM model that are common to both the LM2009 version without crossflow and the LM2015 version with crossflow effects. The compressibility correction for $Re_{\theta t}$ has the form $(Re_{\theta t})_{New} = (Re_{\theta t})_{Original}$. $F(M_e)$, where the correction term $F(M_e)$ is a function of the local edge Mach number and is evaluated via an analytical curve fit derived from the results of stability computations by Masad and Malik [75] and Masad and Abid [76].

The performance of the compressibility-corrected LM model was evaluated for several canonical 2D and 3D configurations, including a flat plate, the RAE (NPL) 5212 and NLR 7301

supercritical airfoils, and the CRM-NLF wing. Figure 18(a) illustrates the increasing underprediction of the transition Reynolds number by the baseline LM model over an adiabatic flat plate as the freestream Mach number increases from 0.0 to 1.4. Figures 18(a) and 18(b) confirm that the above discrepancy is substantially reduced by the compressibility correction, resulting in improved predictions of transition onset up to the transonic regime.





- (a) Transition onset Reynolds number, Ret
- (b) C_f distribution at M = 1.2

Figure 18 - Influence of Mach number on the transition onset Reynolds number, Re_t for a flat plate, as predicted by stability analysis (N_{crit} = 9) and the LM2009 model (Tu = 0.07%), respectively. Skin-friction evolution over a flat plate as predicted by the original LM2009 transition model and with corrections to account for compressibility effects. The vertical black lines mark the predicted transition location based on stability correlation.

Surface pressure distributions for the supercritical RAE (NPL) 5212 airfoil for selected combinations of Mach number and angle of attack are shown in Fig. 19. The C_p distribution for M = 0.5, $\alpha = 0.0^{\circ}$ (Fig. 19(a)) indicates a narrow region of stronger adverse gradient immediately behind the suction peak, followed by an extended region of milder adverse pressure gradient. A similar behavior is also noted for the case with M = 0.7 and $\alpha = 1.35^{\circ}$ in Fig. 19(b), indicating a potentially non-self-similar boundary layer in each of these cases. Despite the O(1) Mach numbers, the transition locations predicted by the baseline LM2009 model compare well with the stability-based CFD predictions including compressibility effects. In contrast, however, the baseline LM2009 model predicts significantly earlier transition than the PSE analysis for the case with M = 0.75 and $\alpha = 0.0^{\circ}$ (Fig. 19(c)), which includes an extended region of favorable pressure gradient. Including the compressibility correction (red curves) in the LM2009 results in a downstream transition location due to shock-induced separation, similar to the predictions of the stability theory.

The CRM-NLF swept-wing configuration from Section 3.2 was also investigated to assess the performance of the LM family of models for a complex, 3D configuration. Figure 20 compares the transition fronts predicted by the original and compressibility-corrected versions of the LM2015 model with the inferred transition front from the TSP data [43]. The corrected model shows significantly better agreement with the experimental data in the mid-span region (0.6 m < y < 1.2 m), as well as shifting the transition front in the inboard region closer to the data inferred from the TSP image.

In summary, for attached boundary layers without persistent adverse pressure gradients, the proposed compressibility correction based on linear stability theory led to significantly improved transition onset predictions in the high-subsonic to transonic regime. Its notable features include an automatic deactivation at low Mach numbers, which preserves the underlying calibration based on low-speed flows, and a local formulation for easy implementation in RANS-based flow solvers.

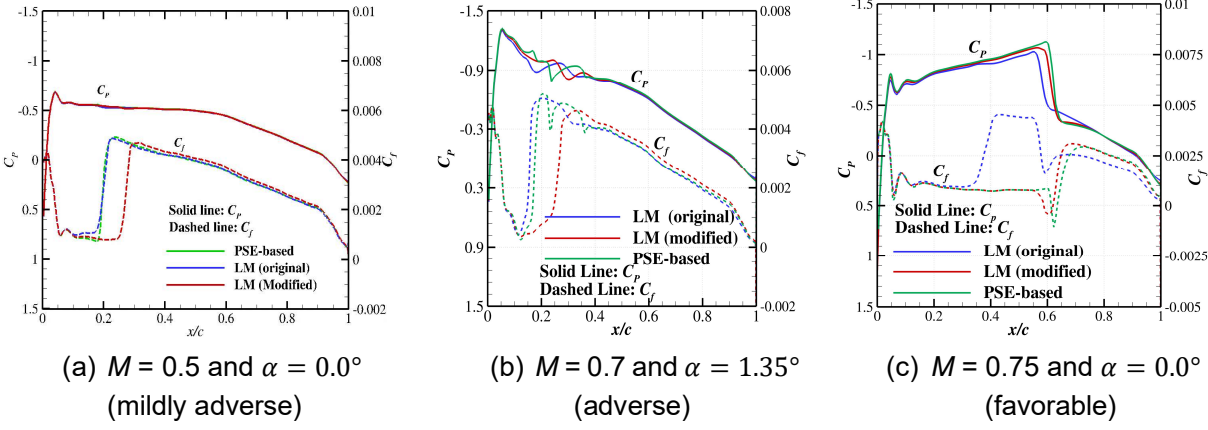


Figure 19 - Predicted distribution of C_p and C_f on the upper surface of the RAE (NPL) 5212 airfoil for $Re_c = 7.5 \times 10^6$. Based on Mack's correlation [73], Tu = 0.07% in all cases to be consistent with $N_{tr} = 9$ for the PSE analysis.

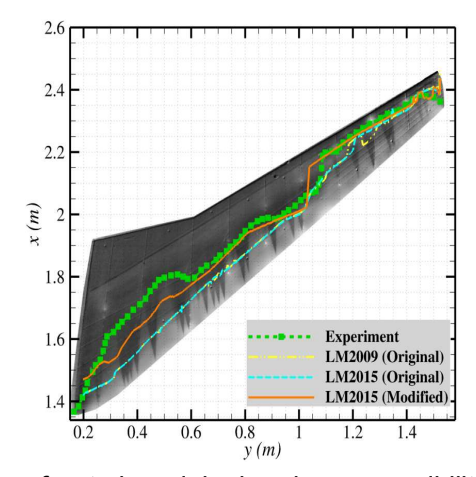


Figure 20 - Predicted transition fronts by original and compressibility-corrected LM2015 models with TSP image and inferred transition front for the CRM-NLF at $\alpha=1.44^{\circ}$, M=0.856, Tu=0.12%, and $Re_{MAC}=15\times10^{6}$ (where *MAC* refers to mean aerodynamic chord).

4.4 Maturation of Transport-Based Transition Models for Hypersonic Flows

As mentioned in the previous section, the majority of transport-based transition models were initially developed for low-speed flows. Their adaptation to supersonic and hypersonic regimes began significantly later, causing the high-speed versions to be less mature at this point. Recently, a number of extensions for hypersonic flows have been suggested in the literature, such as those in Refs. [18] – [21]. However, most of these models have not been widely adopted beyond the groups that originally developed them. One exception to this trend is the SST- γ model of Liu et al. [20] that has been implemented by multiple research groups [77]. To a lesser extent, the SST- γ - ν _L model of Qiao et al. [19] has also received some scrutiny in our work [78]. Another obstacle to the broader adoption of transition models for high-speed flows is the increased physical complexity of both the high-speed mean flows and the associated transition processes. This complexity also necessitates a greater level of detail in the model specification. To facilitate the maturation of transport-based transition modeling for high-speed flows, the abovementioned SST- γ and SST- γ - ν _L models have been selected for further study. Both models have been implemented in NASA's OVERFLOW 2.3 RANS CFD solver [78] to enable further assessment. Their porting to the FUN3D solver is currently in progress.

The grid convergence characteristics of each model for a 5-degree half-angle cone at flow conditions from the experiments by Horvath et al. [56] are illustrated in Figs. 21 and 22. Figures 21(a)-21(c) display the integrated heat loads across the laminar, transitional, and fully turbulent regions, respectively. The spatial extents of all three regions are chosen to be the same for both models. For

this test case, the laminar region extends from the nose of the cone to an axial distance of 0.175 m, the transitional region encompasses the region x = [0.175 m, 0.4 m], and the turbulent region is comprised of the remaining portion of the cone downstream of x = 0.4 m. For each metric, the plots also indicate the asymptotic predictions in the limit of $h \to 0$ (where $h = N_{tot}^{-1/2}$, N_{tot} being the total number of grid points in the 2D mesh), obtained through Richardson extrapolation. This study marks the first time in the literature that the formal grid convergence properties of transition models have been examined for hypersonic flows. All three scalar metrics indicate a satisfactory convergence to their asymptotic values. It's also seen that the heat load across the transition zone converges rather quickly for the SST-y-v model, whereas significantly finer meshes are necessary for the SST-y solutions to approach their asymptotic limit. This trend is confirmed by the comparison of Stanton number distributions for multiple grid levels in Fig. 22. Figure 22(a) also reveals that the relatively rapid rise in heat transfer following the onset of transition is followed by an extended slow rise such that the peak turbulent heat transfer is not achieved for a considerable distance downstream of the transition onset location. This anomalous behavior of the SST-y solution accounts for the lower value of heat load within the transitional region as seen from Fig.21(b). By contrast, the SST-y-v model predicts lower values of surface heating in the fully turbulent region than the predictions of the SST turbulence model with no transition model, as seen in Fig. 21(c). This issue as well as other details of the two hypersonic transition model implementations are further discussed in Refs. [73] and [80].

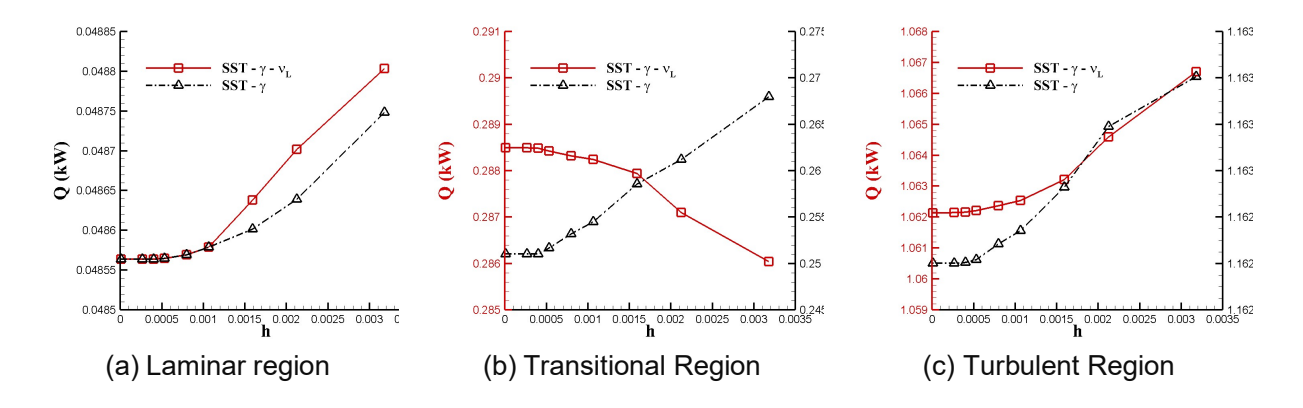
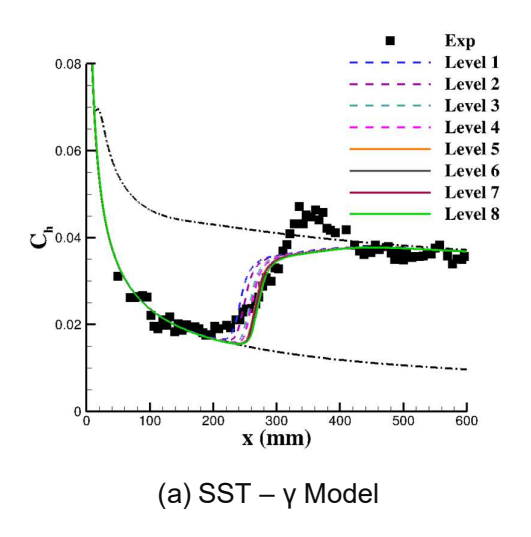


Figure 21 - Convergence of the surface heat transfer in the laminar, transitional, and turbulent regions for the LaRC 20-in Mach 6 test case ($Re = 14.1 \times 10^6$ /m) using the SST- γ and SST- γ - ν L models. In this figure, $h = N_{tot}^{-1/2}$, where N_{tot} corresponds to the total number of grid points in the 2D mesh.

4.5 Verification of Transition Models

Uncertainty quantification is particularly important for transition modeling, due to the sensitivity of the transition process to small variations in flow conditions, geometry, and surface roughness. In that regard, model verification is an essential component of transition modeling research, as it helps ensure that the implemented transition model equations are being solved accurately and consistently and that the solutions obtained using different solvers match in the limit of vanishing error due to discretization. Model verification is, therefore, a crucial pre-requisite to model validation. Given the increasing use of RANS-based transition models, recent workshops by AIAA (1st AIAA Transition Prediction and Modeling Workshop) and NATO (AVT-313 working group) have focused on community wide assessments of these models. An important finding from these workshops [81] was that, even for simple configurations, there was a significant scatter amongst the results computed using different flow solvers that purportedly used the same transition model. These discrepancies persisted even when the same grid family was utilized, and even as the grid was systematically refined within a given family. Such inconsistencies highlight the urgent need for transition model verification, as the lack thereof precludes the quantification of errors associated with a given model and, hence, its validation against the benchmark data.



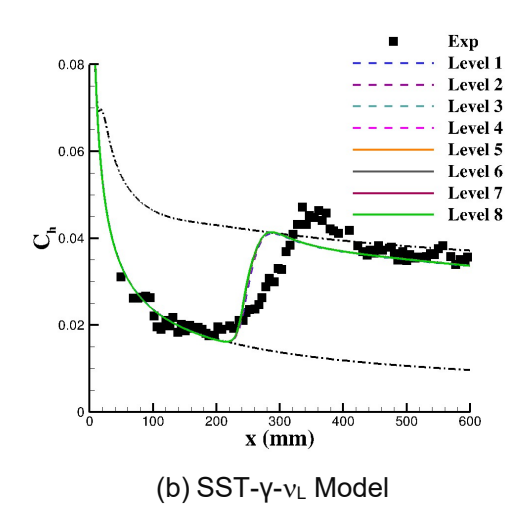


Figure 22 - Convergence of the axial distributions of surface Stanton number C_h for the case from Fig. 19. Mesh level 8 is the finest mesh considered and the resolution along each spatial direction doubles across every other level. For reference, each figure also indicates the predictions based on fully laminar and fully turbulent solutions.

To help CFD code developers verify their implementations of the transition models, Venkatachari et al. [82] applied the SST2003-LM2009 model in OVERFLOW and FUN3D flow solvers to selected canonical configurations from the AIAA Workshop,² namely, a flat-plate case (T3A) with bypass transition and the NLF(1)-0416 airfoil at conditions involving both natural and separationinduced transition scenarios, along with an additional flat-plate case with natural transition on the flat plate. Cross-comparisons of surface distributions of pressure and skin-friction coefficients were made. Richardson extrapolation was used to estimate the grid converged values of several scalar metrics, including the drag coefficients (and lift coefficient for the airfoil case), along with point values of the skin-friction coefficient C_f at selected locations. With the exception of the C_f value in the transition zone in two cases, all scalar metrics predicted by the two codes were found to converge to nearly the same values, even with different numerical methods (finite volume vs finite difference) and different orders of discretization for the convective fluxes, etc. Because the underlying turbulence model (SST-2003) in these solvers has already been verified in previous work, the above findings provide an encouraging prognosis for removing the dependence of transition model predictions on the flow solver, thus creating the foundation for meaningful code to code comparisons in future workshops, and also, for validating the transition models or specific aspects of those models.

Figure 23 from Ref. [82] illustrates the grid convergence of both global and local flow metrics for an NLF(1)-0416 airfoil at $\alpha=5^{\circ}$ ($M_{\infty}=0.1$, $Re_{c}=4\times10^{6}$, Tu=0.15%, and $T_{\infty}=300$ K). Under these conditions, the upper surface boundary layer is fully attached and transitions due to TS instabilities. On the other hand, the lower surface flow exhibits a short separation bubble that transitions prior to reattachment.

Figures 23(a) and 23(b) indicate that the lift and drag coefficients converge fairly rapidly as the grids are refined, with mesh 6 (denoted by the fifth square and circle from the left in each curve) enabling predictions that might be considered acceptable during practical calculations. However, the local skin-friction coefficient in the transition zone shows significantly slower convergence, which is primarily a result of the continued shift in transition onset location as the mesh gets refined. The grids provided by the organizers of the AIAA 1st CFD Transition Modeling Workshop were designed for general use, without any adaptation to specific conditions. As seen from the results in Fig. 23, this approach requires rather fine meshes (mesh counts of O(10⁷) for level 10) to achieve code-independent asymptotic predictions.

-

² https://transitionmodeling.larc.nasa.gov/workshop i/

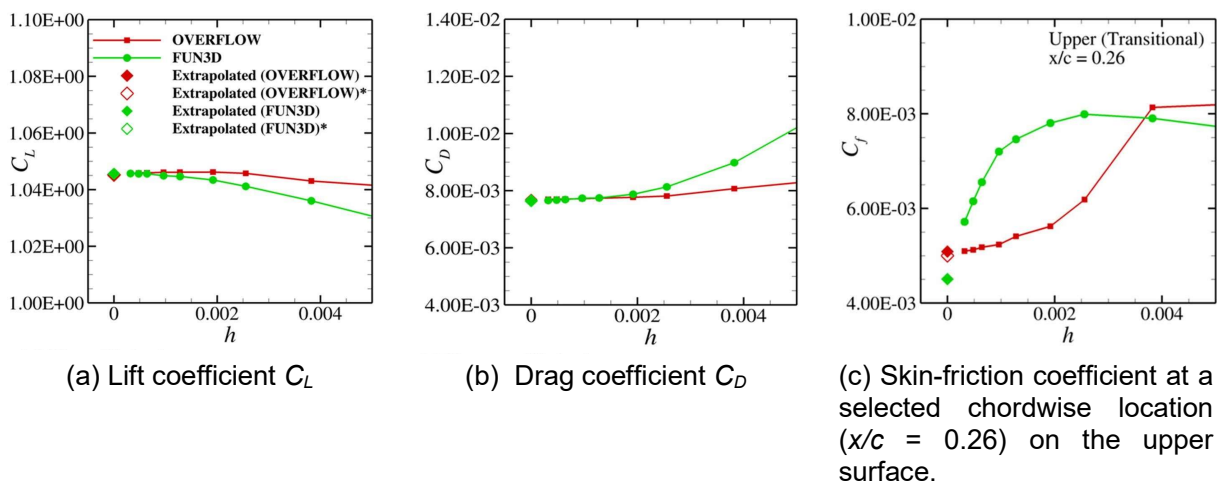


Figure 23 - Grid convergence characteristics of both global and local flow metrics obtained using LM2009 implementations in the OVERFLOW and FUN3D solvers. The benchmark case corresponds to an NLF(1)-0416 airfoil at $\alpha=5^\circ$ (M=0.1, $Re_c=4\times10^6$, Tu=0.15%); Open diamond symbol: extrapolated solution obtained using mesh levels 7, 8, and 9; closed diamond symbol: extrapolated solution obtained using mesh levels 8, 9, and 10, the latter being the finest mesh level (i.e., leftmost square or circle in each plot). The cell count along each coordinate direction doubles every other level, with approximately 11 million grid points in the finest mesh (level 10). These results are based on using turbulence sustaining terms to prevent numerical decay of freestream turbulence.

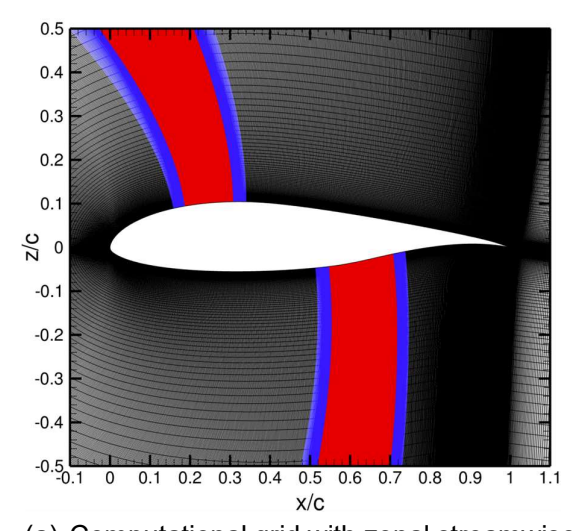
Even though satisfactory grid convergence could be achieved for the 2D canonical flows in [82], it required mesh counts that are substantially larger than those used in typical applications. Thus, further efforts are necessary to reduce the mesh sizes, particularly to enable similar computations for fully 3D configurations. As a first step, we have applied different structured and unstructured grid refinement strategies to better understand the accuracy, convergence, and performance of the Langtry-Menter γ - Re_{θ_t} model for 2D configurations with both natural and separation-induced transition [83]. These strategies include structured streamwise refinement near transition zones as opposed to expensive globally uniform refinement, metric-based unstructured grid adaptation, and adjoint-based grid adaptation.

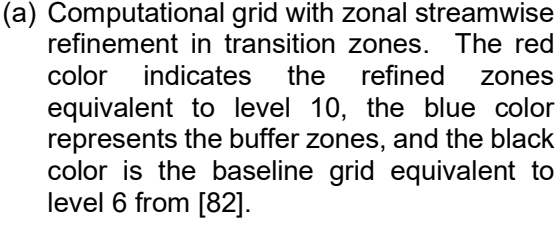
The results of these computations suggest that streamwise refinement just within the transition zone (Fig. 24(a)) may yield significant savings in capturing the separation-bubble-induced transition, provided the wall-normal grid exceeds a certain threshold. Figure 24(b) shows that using a computational mesh with a wall-normal baseline level of 10 and a streamwise baseline level of 6 with zonal streamwise refinement that is locally equivalent to a level 10 baseline mesh is identical to the LSB solution obtained with a globally refined level 10 baseline mesh that is more than 3 times as large.

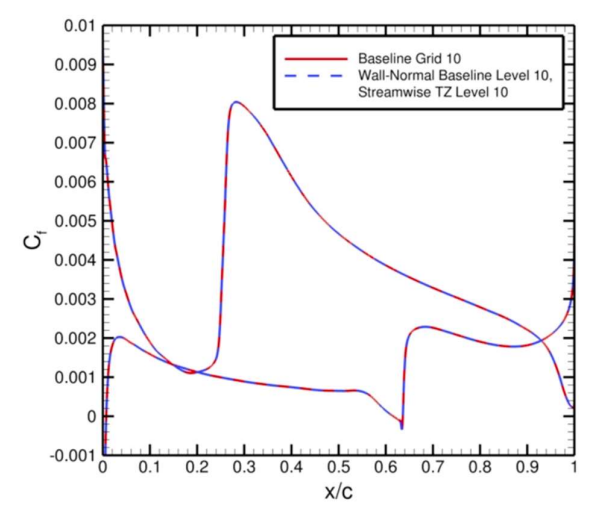
Two additional strategies were explored toward automated grid refinement for transition-model computations. Strategy 1 focused on metric-based unstructured grid adaptation via the *refine* library from the FUN3D solver. Although computations of natural and separation-induced transition on the NLF-0416 airfoil showed plateauing of both lift and drag coefficients at significantly lower mesh sizes, the apparently converged transition locations differed notably from the onset locations obtained using the globally refined structured grid family. We believe that this inaccuracy stems from the poor nearwall resolution due to the use of the Mach number Hessian as the sole metric for grid adaptation and that addressing this shortcoming via improved adaptation metrics should significantly improve the overall efficacy of metric-based adaptation for transition computations based on transport equations.

Adjoint-based grid adaptation was also explored in Ref. [83]. Because the adjoint capability in the FUN3D solver does not yet include the transition models, the NLF-0416 airfoil case with imposed transition with the SA turbulence model was used to assess the efficacy of the adjoint grid adaptation to manage the flow field variations in a generic transitional flow. The adjoint-based strategy provided clear improvements in the near-wall resolution of the adapted grid and yielded predictions that were in closer agreement with the reference solution in comparison with a comparable size mesh

obtained via uniform refinement of a baseline unstructured grid. This highlights the need to extend the adjoint capabilities to include transition models.







(b) Comparison between C_f distributions on a fine baseline grid and transition-zone refined grid from part (a).

Figure 24 - Efficacy of zonal streamwise refinement in transition zones over an NLF-0416 airfoil at $\alpha = 5^{\circ}$ (M = 0.1, $Re_c = 4 \times 10^6$, Tu = 0.15%).

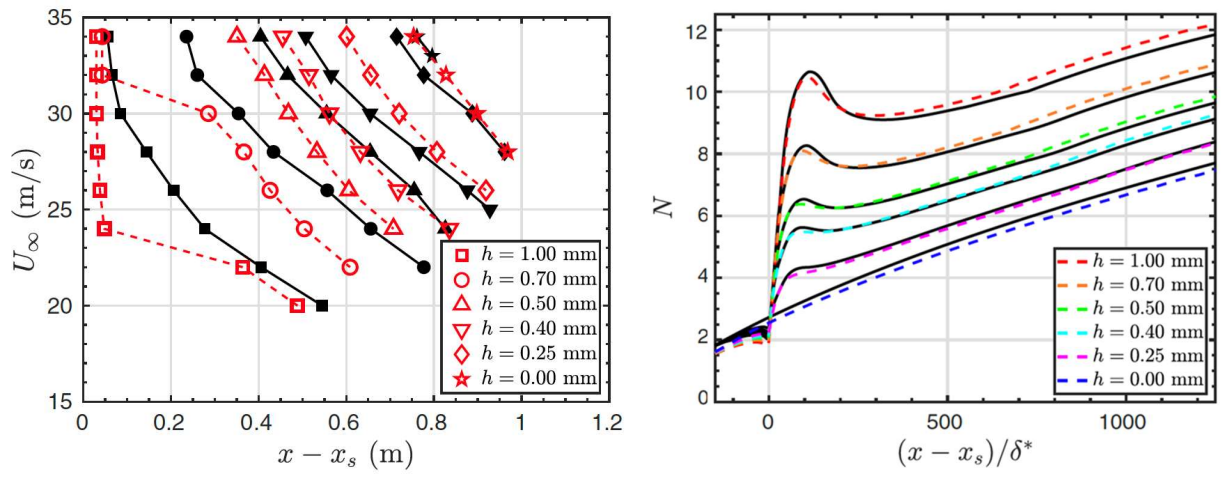
Overall, this work on adaptive mesh solutions has emphasized the importance of grid design during model verification. It has contributed useful insights into the strengths and shortcomings of the existing mesh adaptation capabilities in FUN3D and highlighted the need for further development, particularly with respect to improved automated adaptation strategies for viscous flows. To that end, it would be useful to pursue hybrid, solution-adaptive grids that smoothly integrate near-surface prismatic layers with unstructured meshes away from the surface.

4.6 Effect of Short-Scale Surface Nonuniformities on Transition Onset

While transition correlations based on the local momentum thickness Reynolds number, Re_{θ} , can be easily integrated into the CFD process via the LCTM approach, they appear to encounter difficulties with problem classes where the cumulative effects of disturbance history are important. One example from our recent experience involves localized surface perturbations, such as steps, gaps, and protuberances, where the basic flow relaxes to the unperturbed flow behind the surface inhomogeneity, but the fluctuation amplitudes continue to carry the memory of disturbance history from the region of mean flow modification due to the excrescence. Accurate modeling of the excrescence effects is important for predicting laminar-turbulent transition on operational aerodynamic surfaces and, hence, to provide an optimal specification of manufacturing tolerances.

In general, the localized excrescence does not alter the underlying transition mechanism unless the excrescence height becomes sufficiently large. Until then, the main effect of the local perturbation is simply a forward movement of the transition onset location due to a net increase in disturbance amplification in the vicinity of the excrescence. Figure 25(a) from Hildebrand et al. [84] illustrates the comparison of LST-based transition onset prediction with experimental measurements by Wang and Gaster [85] for a backward facing step (BFS) of height h. Note that, in the current section, h denotes the step height and not the measure of average grid size as used in the previous section. There is good agreement between the predicted transition onset locations and the corresponding measurements over a broad range of wind tunnel speeds and BFS heights, collectively representing nondimensional steps heights up to about $h/\delta^* < 1.5$. The LST-based transition model directly

accounts for the changes in the laminar basic state due to the BFS and how those changes influence the transition process, while being easily amenable to CFD-integrated transition prediction as discussed earlier. Even though LST cannot capture the nonparallel effects associated with the stronger streamwise gradients near the BFS, a comparison with the disturbance growth predictions based on Harmonic Linearized Navier-Stokes Equations (HLNSE) indicates satisfactory agreement between the respective predictions of N-factor envelopes at various BFS heights (Fig. 25(b)). Figure 25(a) also reveals that the accuracy of LST-based transition predictions degrades at large nondimensional step heights (i.e., higher freestream speeds and/or larger values of h) that advance the onset of transition to the vicinity of the reattachment location behind the step.



(a) Transition locations from LST with N_{tr} = 7.32 (red open symbols/dashed lines) compared with the experimental measurements [85] (black closed symbols/solid lines) for U_{∞} = 20–34 m/s.

(b) Comparison of N-factor envelopes based on LST (dashed lines) and PSE/HLNSE (solid lines) for U_{∞} = 34 m/s.

Figure 25 - Effect of a backward facing step on the transition onset location and the disturbance growth in a flat plate boundary layer for step heights of h = 0-1 mm. Reproduced from Ref. [84].

In stark contrast to the abovementioned findings from stability-based models, transport-equations-based transition models, such as the LM2009 and AFT2019b, fail to accurately predict the shift in transition onset due to the BFS as seen from Figs. 26(a) and 26(b), respectively. Computations have indicated that the LM2009 model indicates virtually no effect of the BFS until the step height becomes rather large when transition onset flashes back to the step location. We believe that because this model relies on a local comparison of the surrogate momentum thickness with the critical momentum thickness, it is apparently unable to provide an adequate account of the history effects related to increased disturbance amplification near the BFS. When transition occurs far downstream of the BFS, the model does not retain the memory of the step-induced perturbation, leading to inaccurate predictions. The AFT2019b model attempts to account for the flow history effects by solving a transport equation for the amplification factor, but it was still unable to predict the measured shift in transition location as a function of BFS height. Similar to LM2009, the AFT2019b model predicted nearly the same transition locations over a significant change in BFS heights; in fact, the AFT-based transition locations for moderate step heights were downstream of the predicted transition onset for the no-step case (*h* = 0 mm).

5. Concluding Remarks

Uncertainty in transition prediction leads to longer design cycles, resulting in suboptimal designs for energy efficient aircraft that lead to higher fuel burn. According to the CFD Vision 2030 report [1], improved transition modeling is also essential to unlocking the full potential of affordable, eddy-resolving WMLES simulations for aircraft analysis and design. Development of accurate, robust, and computationally efficient models is critical to reducing the reliance on costly direct simulations of the transition process. This paper has provided an overview of the recent effort in implementing CFD-

integrated transition models in NASA's OVERFLOW and FUN3D flow solvers. The implementation and assessment of both nonlocal, yet physics-based models rooted in the linear stability paradigm and local correlation-based transition models (LCTMs) encapsulated in auxiliary transport equations were discussed. While not a mature capability as yet, the flexible framework implemented in these solvers should prove valuable to the CFD users.

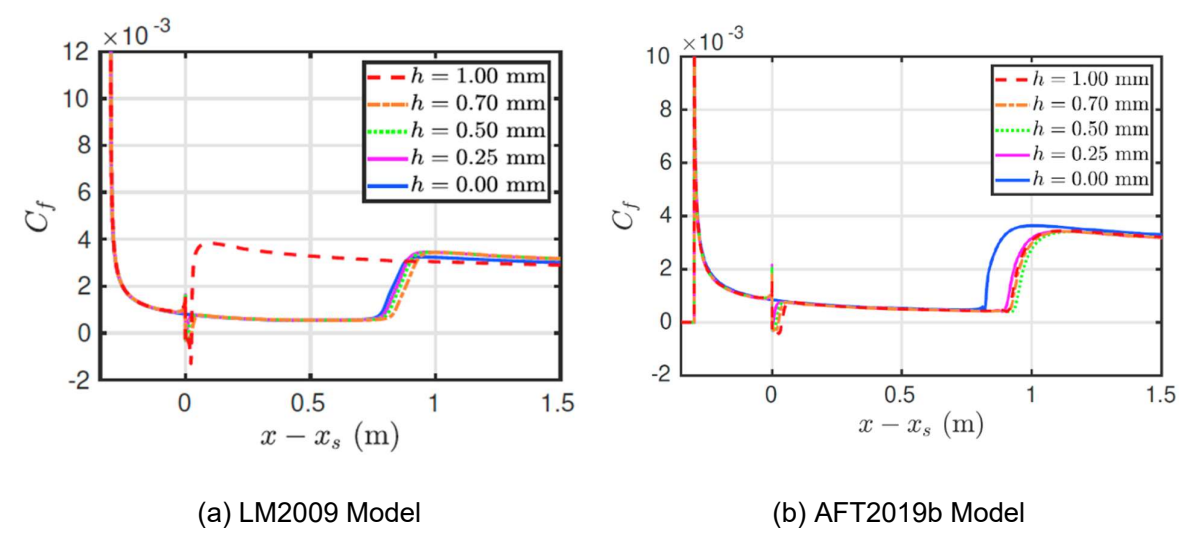


Figure 26 - Transport-equation-based predictions of skin friction along the bottom wall for boundary-layer flow over a BFS with a slope of 75 degrees for U_{∞} = 34 m/s and h = 0–1 mm [104]. Inflow conditions for both models are tuned to match the baseline results (h = 0 mm) with the measured transition location. Reproduced from Ref. [84].

The findings presented in this overview highlight the current limitations of stability-based transition modeling and emphasize the need for continued research to develop more robust transition prediction methods that are applicable to a broad range of flows with different transition mechanisms and the significant parameter dependencies of those mechanisms. In general, the need to calibrate the dual N-factor criterion on a case-by-case basis is a notable limitation of the transition models based on linear stability characteristics. After Menter introduced the LCTM concept to facilitate transition modeling using distributed computations with potentially unstructured-grid CFD solvers, significant efforts have been made by a number of researchers to further develop this class of transition models. However, the case studies presented in this paper have underscored the fact that, due to the inherent empiricism in these models and the diverse transition mechanisms encountered in aerospace applications, along with several modifiers for each of those mechanisms, a number of significant shortcomings still need to be addressed. This makes it essential to have the dual as well as diverse capability for transition modeling, at least until the physical basis of the transport-equations-based models can be improved to address the range of key transition scenarios.

We note that both classes of models may encounter challenges in cases where two or more physical mechanisms are simultaneously active and jointly contribute to the transition process, such as TS waves and stationary crossflow instabilities, or TS and traveling crossflow, or second mode and crossflow in high Mach number boundary layers. While empirical fixes exist to deal with mixed transition mechanisms, they need significant calibration based on the flow as well as facility disturbance environment. Data-driven models, such as those based on deep learning approaches, have the potential to tackle these shortcomings. However, past transition measurements do not provide the essential data to validate and improve the transition models. The intrinsic variety of transition mechanisms requires experimental measurements that span the relevant transition mechanisms and are sufficiently detailed, both in terms of characterizing the input forcing and the flow response. Some of the largest gaping holes in the existing data pertain to flows where multiple transition mechanisms can be active either side by side or in concert with each other, and to high-speed boundary layers. In the context of subsonic transports, it is crucial to obtain measurements on configurations with various transition mechanisms, such as swept-wing configurations where both Tollmien-Schlichting (TS) and crossflow instability mechanisms can play a crucial role in transition.

These measurements should identify the primary transition mechanism, provide adequate characterization of the freestream and surface disturbance environment, and explore how variations in both disturbances influence the transition behavior.

Ideally, these experiments should provide a comprehensive dataset covering a range of freestream disturbance environments and surface roughness characteristics. Validation of transition models will also require carefully designed experiments that provide detailed measurements of the transition process, including the onset location, intermittency, and the spatial evolution of turbulent spots. Preferably, these measurements should span a range of flow conditions and geometries relevant to aerospace applications. Of course, with continued increases in compute power, there is also an opportunity to reduce this data gap by supplementing the experimental data with high-fidelity simulations based on a realistic disturbance environment. Advanced data assimilation techniques to combine experimental measurements with CFD simulations [86], accounting for the uncertainties in both, would also play an important role in the validation of transition models. Realizing the vision of robust, reliable, and physics-based transition modeling in 2030 will require a coordinated effort combining advanced HPC capabilities, targeted experiments, and data-driven model development.

6. Acknowledgments

This research was carried out in support of the Revolutionary Computational AeroSciences discipline under the Transformational Tools and Technologies project of the NASA Transformative Aeronautics Concepts Program. The hypersonic transition modeling work described in Sections 3.4 and 4.4 represents an extension of the TTT funded effort and it has been supported by NASA's Hypersonic Technology project. The authors greatly appreciate computational resources from the K midrange computing cluster at NASA Langley Research Center as well as from the NASA High-End Computing Program through the NASA Advanced Supercomputing Division at the NASA Ames Research Center. We would also like to thank several members of the OVERFLOW, FUN3D, and VULCAN-CFD development teams for their valuable assistance throughout this effort. Collaborations with the NASA Langley teams involved in the CRM-NLF and Juncture Flow experiments and with Prof. Heng Xiao (previously at Virginia Tech) are gratefully acknowledged.

7. Contact Author Email Address

The corresponding author of the present paper can be contacted at the following email address: m.m.choudhari@nasa.gov

8. Copyright Statement

The authors confirm that this material is a work of the U.S. Government and is not subject to copyright protection in the United States. The authors also confirm that they have obtained permission, from the copyright holder of any third party material included in this paper, to publish it as part of their paper. The authors confirm that they give permission, or have obtained permission from the copyright holder of this paper, for the publication and distribution of this paper as part of the ICAS proceedings or as individual off-prints from the proceedings.

References

- [1] Slotnick, J., Khodadoust, A., Alonso, J., Darmofal, D., Gropp, W., and Mavriplis, D., "CFD Vision 2030 Study: A Path to Revolutionary Computational Aerosciences," NASA/CR-2014-218178, 2014. https://ntrs.nasa.gov/citations/20140003093.
- [2] Smith, A. M. O. and Gamberoni, N., "Transition, Pressure Gradient and Stability Theory," Douglas Aircraft Company, Long Beach, Calif. Rep. ES 26338, 1956. https://engineering.purdue.edu/~aae519/BAM6QT-Mach-6-tunnel/otherpapers/smith-amo-eN-douglas-es26388-1956.pdf.
- [3] van Ingen, J. L., "A Suggested Semi-Empirical Method for the Calculation of the Boundary Layer Transition Region," University of Delft, Dept. of Aerospace Engineering, Delft, The Netherlands, Rep. VTH-74, 1956. http://resolver.tudelft.nl/uuid:cff1fb47-883f-4cdc-ad07-07d264f3fd10.
- [4] Drela, M. and Giles, M. B., "Viscous-Inviscid Analysis of Transonic and Low Reynolds Number Airfoils," *AIAA Journal*, Vol. 25, No. 10, 1987, pp. 1347–1355. https://doi.org/10.2514/3.9789

- [5] Arnal, D., Casalis, G., and Houdeville, R., "Practical Transition Prediction Methods: Subsonic and Transonic Flows," AVT-151RTOAVT/ VKI Lecture Series, No. 8, Von Karman Inst., Rhode-Saint-Genèse, Belgium, 2008.
- [6] Perraud, J., Arnal, D., Casalis, G., Archambaud, J.-P., and Donelli, R., "Automatic Transition Predictions Using Simplified Methods," *AIAA Journal*, Vol. 47, No. 11, 2009, pp. 2676–2684. https://doi.org/10.2514/1.42990
- [7] Campbell, R., Campbell, M., and Streit, T., "Progress Toward Efficient Laminar Flow Analysis and Design", AIAA 2011-3527. https://doi.org/10.2514/6.2011-3527
- [8] Davis, M. B., Reed, H. L., Youngren, H., Smith, B., and Bender, E., "Transition Prediction Method Review Summary for the Rapid Assessment Tool for Transition Prediction (RATTraP)," Technical Report AFRL-VA-WP-TR-2005-3130, Air Force Research Lab, Wright-Patterson AFB, OH, 2005.
- [9] Menter, F. R., Langtry, R. B., and Völker, S., "Transition Modelling for General Purpose CFD Codes," J. Flow, Turbulence and Combustion, Vol. 77, 2006, pp. 277–303. https://doi.org/10.1007/s10494-006-9047-1
- [10] Menter, F. R., Kuntz, M., and Langtry, R., "Ten Years of Industrial Experience with the SST Turbulence Model," *Turbulence, Heat and Mass Transfer*, Vol. 4 (1), 2003, pp. 625–632. http://cfd.mace.manchester.ac.uk/flomania/pds papers/file pds-1068134610Menter-SST-paper.pdf
- [11] Langtry, R. B. and Menter, F. R., "Correlation-Based Transition Modeling for Unstructured Parallelized Computational Fluid Dynamics Codes," *AIAA Journal*, Vol. 47, No. 12, 2009, pp. 2894–2906. https://doi.org/10.2514/1.42362
- [12] Menter, F. R., Smirnov, P. E., Liu, T., and Avancha, R., "A One-Equation Local Correlation-Based Transition Model," *Flow, Turbulence and Combustion*, Vol. 95, Issue 4, Dec. 2015, pp. 583–619. https://doi.org/10.1007/s10494-015-9622-4
- [13] Walters, D. K., and Cokljat, D., "A Three-Equation Eddy-Viscosity Model for Reynolds-Averaged Navier—Stokes Simulations of Transitional Flow," Journal of Fluids Engineering, Vol. 130, No. 12, 2008, 121401. https://doi.org/10.1115/1.2979230
- [14] Spalart, P. R. and Allmaras, S. R., "A One-Equation Turbulence Model for Aerodynamic Flows," *Recherche Aerospatiale*, No. 1, 1994, pp. 5–21. https://doi.org/10.2514/6.1992-439
- [15] Coder, J. G. and Maughmer, M.D., "Computational Fluid Dynamics Compatible Transition Modeling Using an Amplification Factor Transport Equation," *AIAA Journal*, Vol. 52, No. 11, 2014, pp.2506–2512. https://doi.org/10.2514/1.J052905
- [16] Langtry, R. B., Sengupta, K., Yeh, D. T., and Dorgan, A. J., "Extending the γ-Re_{θt} Correlation based Transition Model for Crossflow Effects," AIAA Paper 2015-2474, 2015. https://doi.org/10.2514/6.2015-2474
- [17] Grabe, C., Shengyang, N., and Krumbein, A., "Transport Modeling for the Prediction of Crossflow Transition," AIAA Journal, Vol.56, 2018, pp.3167–3178. https://doi.org/10.2514/1.J056200
- [18] Xu, J., Bai, J., Fu, Z., Qiao, L., Zhang, Y., and Xu, J., Parallel Compatible Transition Closure Model for Highspeed Transitional Flow," AIAA Journal, Vol. 55 (9), 2017, pp. 3040–3050. https://doi.org/10.2514/1.J055711.
- [19] Qiao, L., Bai, J., Xu, J., Xu, J., and Zhang, Y., "Modeling of Supersonic/Hypersonic Boundary Layer Transition Using a Single-Point Approach," *International Journal of Nonlinear Sciences and Numerical Simulation*, Vol. 19(3-4), 2018, pp. 263–274. https://doi.org/10.1515/ijnsns-2017-0011.
- [20] Liu, Z., Lu, Y., Li, J., and Yan, C., "Local Correlation Based Transition Model for High-Speed Flows," *AIAA Journal*, Vol. 60(3), 2022, pp. 1365–1381. https://doi.org/h10.2514/1.J060994.
- [21] Liu, Z., Lu, Y., Xiao, F., and Y, C., "Further Developments to a Local Correlation-Based Transition Model for Hypersonic Flows," *AIAA Journal*, Vol. 60(6), 2022, pp. 3909–3916. https://doi.org/10.2514/1.J061585.
- [22] Nichols, R. H, and Buning, P. G., "User's Manual for OVERFLOW 2.3, Version 2.3," NASA Langley Research Center, Hampton, VA, Oct 2019. https://overflow.larc.nasa.gov/home/users-manual-for-overflow-2-3.
- [23] Anderson, W. K., Biedron, R. T., Carlson, J.-R., Derlaga, J. M., Druyor, C. T., Gnoffo, P. A., Hammond, D. P., Jacobson, K. E., Jones, W. T., Kleb, B., Lee-Rausch, E. M., Nastac, G. C., Nielsen, E. J., Park, M. A., Rumsey, C. L., Thomas J. L., Thompson, K. B., Walden, A. C., Wang L., Wood S. L., Wood, W. A., Diskin, B., Liu, Y. and Zhang, X., "FUN3D Manual: 14.0," NASA TM-20220017743, 2022, https://fun3d.larc.nasa.gov/papers/FUN3D INTG Manual-14.0.pdf.
- [24] Baurle, R., White, J., Drozda, T., and Norris, A. "VULCAN-CFD theory manual: Ver. 7.1.0," NASA TM-2020-5000766, 2020.

- [25] Krumbein, A., Krimmelbein, N., Grabe, C., and Shengyang, N., "Development and Application of Transition Prediction Techniques in an Unstructured CFD Code," AIAA Paper 2015-2476, 2015. https://doi.org/10.2514/6.2015-2476
- [26] Aupoix, B., Arnal, D., Bézard, H., Chaouat, B., Chedevergne, F., Deck, S., Gleize, V., Grenard, P., Laroche, E., "Transition and Turbulence Modeling," AerospaceLab Journal, Issue 2, March 2011, pp. 1-13.
- [27] Dagenhart, J. R., and Saric, W. S., "Crossflow Stability and Transition in Swept Wing Flow," NASA TP-1999-209344, 1999.
- [28] Chang, C.-L., "LASTRAC.3d: Transition Prediction in 3D Boundary Layers," AIAA Paper 2004-2542, 2004. https://doi.org/10.2514/6.2004-2542
- [29] Chang, C.-L., "Langley Stability and Transition Analysis Code (LASTRAC) Version 1.2 User Manual," NASA TM-2004-213233, 2004. https://ntrs.nasa.gov/api/citations/20040082550/downloads/20040082550.pdf
- [30] Chang, C.-L., "Development of Physics-Based Transition Models for Unstructured-Mesh CFD Codes using Deep Learning Models," AIAA Paper 2021-2828, 2021. https://doi.org/10.2514/6.2021-2828
- [31] Zafar, M. I., Choudhari, M., Paredes, P., and Xiao, H., "Recurrent Neural Network for End-to-End Modeling of Laminar-Turbulent Transition," *Data-Centric Engineering*, 2021, pp. 1–31. https://doi.org/10.1017/dce.2021.11
- [32] Zafar, M. I., Xiao, H., Choudhari, M. M., Li, F., Chang, C.-L., Paredes, P., and Venkatachari, B., "Convolutional Neural Network for Transition Modeling Based on Linear Stability Theory," *Physical Review Fluids*, 5:113903. https://doi.org/10.1103/PhysRevFluids.5.113903
- [33] Paredes, P., Venkatachari, B., Choudhari, M. M., Li, F., Chang, C.-L., Zafar, M. I., and Xiao, H., "Toward a Practical Method for Hypersonic Transition Prediction Based on Stability Correlations," *AIAA Journal*, Vol. 58(10), pp. 4475–4484, 2020. https://doi.org/10.2514/1.J059407
- [34] Herbert, T., "Parabolized Stability Equations," Annu. Rev. Fluid Mech., 29:245-283, 1997. https://doi.org/10.1146/annurev.fluid.29.1.245
- [35] Malik, M., Liao, W., Lee-Rausch, E., Li, F., Choudhari, M., and Chang, C.-L., "Computational Anaysis of the G-III Laminar Flow Glove," AIAA Paper 2011-3525, 2011. https://doi.org/10.2514/6.2011-3525
- [36] Halila, G. L. O., Chen. G., Shi, Y., Fidkowski, K., Martins, J. R. R. A., and de Mendonça, M. T., "High-Reynolds number transitional flow simulation via parabolized stability equations with an adaptive RANS solver," *Aerospace Science and Technology*, Volume 91, Aug. 2019, pp. 321-336. https://doi.org/10.1016/j.ast.2019.05.018
- [37] Li, F., Berry, S. A., Choudhari, M., and Paredes, P., "Basic State Computations and Stability Analysis for Selected BOLT-II Flight Conditions," Presented in special session on BOLT-II Flight Experiment at AIAA SciTech Forum, National Harbor, MD, Jan. 2023. https://ntrs.nasa.gov/api/citations/20230000474/downloads/Li BOLT II session oral presentation 01
- [38] Leidy, A. N., Kegerise, M. A., Hannon, J. A., Choudhari, M., Venkatachari, B. S., and Paredes, P. A., "Measurements and Computations of Natural Transition on the NASA Juncture-Flow Model with a Symmetric Wing," AIAA Paper 2023-0441, 2023. https://doi.org/10.2514/6.2023-0441

23 NH2.pdf

- [39] Venkatachari, B. S., Paredes, P., Choudhari, M., Li, F., and Chang, C.-L., "Pretest Computational Assessment of Boundary Layer Transition in the NASA Juncture Flow Model with an NACA 0015-Based Wing," AIAA Paper 2021-2502, 2021. https://doi.org/10.2514/6.2021-2502
- [40] Rivers, M. B., Lynde, M. N., Campbell, R. L., Viken, S. A., Chan, D. T., Watkins, A. N., and Goodliff, S. L., "Experimental Investigation of the NASA Common Research Model with a Natural Laminar Flow Wing in the NASA Langley National Transonic Facility," AIAA Paper 2019–2189, 2019. https://doi.org/10.2514/6.2019-2189.c1.
- [41] Lynde, M. N., and Campbell, R. L., "Computational Design and Analysis of a Transonic Natural Laminar Flow Wing for a Wind Tunnel Model," AIAA Paper 2017-3058, 2017. https://doi.org/10.2514/6.2017-3058
- [42] Lynde, M. N., Campbell, R. L., Rivers, M. B., Viken, S. A., Chan, D. T., Watkins, A. N., and Goodliff, S. L., "Preliminary Results from an Experimental Assessment of a Natural Laminar Flow Design Method," AIAA Paper 2019-2298, 2019. https://doi.org/10.2514/6.2019-2298
- [43] Lynde, M. N., Campbell, R. L., and Viken, S. A., "Additional Findings from the Common Research Model Natural Laminar Flow Wind Tunnel Test," AIAA Paper 2019-3292, 2019. https://doi.org/10.2514/6.2019-3292
- [44] Paredes, P., Venkatachari, B., Choudhari, M., and Li, F., "Transition Analysis for the CRM-NLF Wind Tunnel Configuration," AIAA Paper 2023-3532, 2021. https://doi.org/10.2514/6.2021-3532

- [45] Crouch, J., Sutanto, M., Witkowski, D., Watkins, A., Rivers, M., and Campbell, R., "Assessment of the National Transition Facility for Natural Laminar Flow Testing," AIAA Paper 2010-1302, 2010. https://doi.org/10.2514/6.2010-1302
- [46] Paredes, P., Venkatachari, B., Choudhari, M., Li, F., Hildebrand, N., and Chang, C. L., "Transition Analysis for the CRM-NLF Wind Tunnel Configuration," AIAA Paper 2021-1431, 2021. https://doi.org/10.2514/6.2021-1431
- [47] van Dam, C. P., Vijgen, P. M. H. W., Yip, L. P., and Potter, R. C., "Leading-Edge Transition and Relaminarisation Phenomena on a Subsonic High-Lift System," AIAA Paper 93-3140, July 1993. https://doi.org/10.2514/6.1993-3140
- [48] Klausmeyer, S. M., and Lin, J. C., "Comparative Results from a CFD Challenge over a 2-D Three-Element High-Lift Airfoil," NASA TM-112858, 1997.
- [49] Choudhari, M., Bahr, C., Khorrami, M., Lockard, D., Lopes, L., Zawodny, N., Herr, M., Pott-Pollenske, M., Kamruzzaman, M., van de Ven, T., Manoha, E., Redonnet, S., Yamamoto, K., Ikeda, T., Imamura, T., "Simulations & Measurements of Airframe Noise: a BANC Workshops Perspective," Proceedings of NATO STO-MP-AVT-246 Specialists Meeting on Progress and Challenges in Validation Testing for Computational Fluid Dynamics, Avila, Spain, September 26-28, 2016.
- [50] Rumsey, C. L., Gatski, T. B., Ying, S., and Bertelrud, A., "Prediction of High-Lift Flows Using Turbulent Closure Models," *AIAA Journal*, Vol. 36, No. 5, May 1998, pp. 765-774. https://doi.org/10.2514/2.435
- [51] Malik, M. R. and Lin, R. S., "Transition Prediction on the Slat of a High-Lift System," *J. Aircraft*, Vol. 36, No. 5, May 1998, pp. 765-774. https://arc.aiaa.org/doi/pdf/10.2514/1.4165
- [52] Halila, G. L. O., Bigarella, E. D. V., and Azevedo, J. L. F., "A Numerical Study on Transitional Flows Using a Correlation-Based Transition Model," *Journal of Aircraft*, Vol. 53, No. 4, 2016, pp. 922–941. https://doi.org/10.2514/1.C033311
- [53] Hildebrand, N., Li, F., and Choudhari, M., "Transition Prediction for the 30P30N and CRM-HL High-Lift Configurations with FUN3D," To be presented at AIAA SciTech Forum, Jan. 2025.
- [54] Bertelrud, A., "Transition on a Three-Element High Lift Configuration at High Reynolds Numbers," AIAA Paper 98-0703, Jan. 1998. https://doi.org/10.2514/6.1998-0703
- [55] Yip, L. P., Vijgen, P. M. H. W., Hardin, J. D., and van Dam, C. P., "In-Flight Pressure Measurements on a Subsonic Transport High-Lift Wing Section," High-Lift System Aerodynamics, AGARD CP-515, Sept. 1993, pp. 21-1 to 21-9.
- [56] Horvath, T. J., Berry, S. A., Hollis, B. R., Chang, C.-L., and Singer, B. A., "Boundary Layer Transition on Slender Cones in Conventional and Low Disturbance Mach 6 Wind Tunnels," AIAA Paper 2002-2743, 2002. https://doi.org/10.2514/6.2002-2743.
- [57] Tokugawa, N., Choudhari, M., Ueda, Y., Fujii, K., Atobe, T., Li, F., Chang, C.-L., and White, J., "Pressure Gradient Effects on Supersonic Transition over Axisymmetric Bodies at Incidence," *AIAA Journal*, Vol. 53, No. 12, 2015. https://doi.org/10.2514/1.J054070
- [58] Vogel, E. A., Venkatachari, B. S., Li, F., Paredes, P., and Choudhari, M., "CFD Integrated Transition Modeling for High-Speed Flows via Coupled OVERFLOW-LASTRAC Analysis," AIAA Paper 2023-0438, 2023. https://doi.org/10.2514/6.2023-0438.
- [59] Vogel, E. A. and Choudhari M. M. "Enhancements to Linear Stability Solver-Based CFD-integrated Transition Prediction for High-Speed Flows," AIAA Paper 2024-1159, 2024. https://doi.org/10.2514/6.2024-1159
- [60] Kimmel, R., Adamczak, D., Paull, A., Paull, R., Shannon, J., Pietsch, R., Frost, M., and Alesi, H., "HIFiRE-1 Ascent-Phase Boundary-Layer Transition," *Journal of Spacecraft and Rockets*, Vol. 52, No. 1, 2015, pp. 217–230. https://doi.org/10.2514/1.A32851
- [61] Campbell, R. L. and Lynde, M. N., "Natural Laminar Flow Design for Wings with Moderate Sweep," AIAA Paper 2016-4326, 2016. https://doi.org/10.2514/6.2016-4326
- [62] Piotrowski, M. G. H. and Zingg, D. W., "Investigation of a Smooth Local Correlation-based Transition Model in a Discrete-Adjoint Aerodynamic Shape Optimization Algorithm," AIAA Paper 2022-1865, 2022. https://doi.org/10.2514/6.2022-1865
- [63] Lee, J.-D., and Jameson, A., "Natural-Laminar-Flow Airfoil and Wing Design by Adjoint Method and Automatic Transition Prediction," AIAA Paper 2009-0897, 2009. https://doi.org/10.2514/6.2009-897
- [64] Shi, Y., Mader, C. A., He, S., Halila, G. L. O., and Martins, J. R. R. A., "Natural Laminar-Flow Airfoil Optimization Design Using a Discrete Adjoint Approach," *AIAA Journal*, Vol. 58, No. 11, 2020, pp. 4702–4722. https://doi.org/10.2514/1.J058944
- [65] Paredes, P., Mysore, P., Jacobson, K. E., Diskin, B., Hildebrand, N. J., and Choudhari, M., "Aerodynamic Design Optimization for Natural Laminar Flow Airfoils," To be presented at AIAA Aviation Forum, Las Vegas, NV, July 2024.

- [66] Ritter, M., Hilger, J., Ribiero, A.F.P., Öngüt, E., Righi, M., Riso, C., Cesnik, C. E. S., dos Santos, L. G. P., Raveh, D., Drachinsky, A., Stanford, B., Chwalowski, P., Kovvali, R., Singh, B., Düssler, S., Cheng, K. C-W., Palacios, R., Santos, J. P., Marques Jr., F. D., Begnini, G. R., Verri, A. A., Lima, J. J., de Melo, F. B., and Bussamra, F. L., "Collaborative Pazy Wing Analyses for the Third Aeroelastic Prediction Workshop," AIAA Paper 2024-0419, 2024. https://doi.org/10.2514/6.2024-0419
- [67] Venkatachari, B. S., Hildebrand, N. J., Choudhari, M., and Chwalowski, P., "Transition Analysis for the Pazy Wing," AIAA Paper 2023-2685, 2024. https://doi.org/10.2514/6.2024-2685
- [68] Gerakopulous, R., Boutilier, M. S. H., and Yarusevych, S., "Aerodynamic Characterization of a NACA 0018 Airfoil at Low Reynolds Numbers," AIAA Paper 2010-4629, 2010. https://doi.org/10.2514/6.2010-4629
- [69] Ritter, M., Fehrs. M., Mertens, C., "Aerodynamic and Static Coupling Simulations of the Pazy Wing with Transitional CFD for the Third Aeroelastic Prediction Workshop," AIAA Paper 2023-0762, 2023. https://doi.org/10.2514/6.2023-0762
- [70] Coder, J. G., "Further Development of the Amplification Factor Transport Transition Model for Aerodynamic Flows," AIAA Paper 2019-0039, 2019. https://doi.org/10.2514/6.2019-0039
- [71] O'Meara, M. M., and Mueller, T.J., "Laminar Separation Bubble Characteristics on an Airfoil at Low Reynolds Numbers," *AIAA Journal*, Vol. 25, No. 8, 1987, pp.1033-1041. https://doi.org/10.2514/3.9739
- [72] Mertens, C., Guerra, A. G., van Oudheusden, B., Fehrs, M., and Ritter, M. R., "Analysis of the Boundary Layer on a Highly Flexible Wing based on Infrared Thermography Measurements," STAB-Symposium, Berlin, Germany, Nov. 2022. https://doi.org/10.1007/978-3-031-40482-5 1
- [73] Mack, L., "Linear Stability Theory and the Problem of Supersonic Boundary- Layer Transition," *AIAA Journal*, vol. 13, Mar. 1975, pp. 278–289. https://doi.org/10.2514/3.49693
- [74] Venkatachari, B., Paredes, P., Derlaga, J., Buning, P., Choudhari, M., Li, F., and Chang, C.-L., "Assessment of Transition Modeling Capability in OVERFLOW with Emphasis on Swept-Wing Configurations," AIAA Paper 2020-1034, 2020. https://doi.org/10.2514/6.2020-1034
- [75] Masad, J. A. and Malik, M. R., "Transition Correlation in Subsonic Flow over a Flat Plate," *AIAA Journal*, Vol. 31, No. 10, 1993, pp. 1953–1955. https://doi.org/10.2514/3.11872
- [76] Masad, J. A. and Abid, R., "On Transition in Supersonic and Hypersonic Boundary Layers," Int J. Eng. Sci, Vol. 33, No. 13, 1995, pp. 1893–1919. https://doi.org/10.1016/0020-7225(95)00046-Z
- [77] Cutrone, L., Schettino, A., Cardesa, J. I., Delattre, G., Coder, J. G., Qiang, S., Vogel, E., and Choudhari, M., "Transition Prediction in Hypersonic Regime on Complex Geometries with RANS-Based Models," AIAA Paper 2024-0291, 2024. https://doi.org/10.2514/6.2024-0291.
- [78] Vogel, E., Venkatachari, B.S., and Choudhari, M.M., "Evaluation of Transport-Equation-Based Transition Models for High-Speed Boundary Layers Using OVERFLOW," AIAA Paper 2023-3531, June 2023. https://doi.org/10.2514/6.2023-3531
- [79] Vogel, E. A., Choudhari M. M., and Venkatachari B. S., "Assessment and Grid Convergence Study of Transition Models for High-Speed Flows," To be submitted for publication.
- [80] Vogel, E. A., Venkatachari B. S., and Choudhari M. M., "Evaluation of the SST- γ and SST- γ - ν _L Models for Transition in High-Speed Boundary Layers," To be submitted for publication.
- [81] Eça, L., Lopes, R., Toxopeus, S. L., Kerkvliet, M., Bettle, M., Rubino, G., Visonneau, M., Venkatachari, B. S., Hildebrand, N., Choudhari, M. M., Rumsey, C. L., Miozzi, M., Broglia, R., Durante, D., Constantini, M., and Poirier, J. C., "Assessment of Numerical and Modeling Errors of RANS-based Transition Models for Low-Reynolds Number 2-D Flows," 34th Symposium on Naval Hydrodynamics, June, 2022.
- [82] Venkatachari, B. S., Mysore, P. V., Hildebrand, N., Choudhari, M. M., and Denison, M., "Verification of the *γ*-Reθt Transition Model in OVERFLOW and FUN3D," Journal of Aircraft, Vol. 61, No. 2, 2024, pp. 345–364. https://doi.org/10.2514/1.C037445
- [83] Hildebrand, N., Mysore, P. V., Choudhari, M. M., and Paredes, P., "Grid Refinement Techniques for the γ -Re θt Transition Model in FUN3D," AIAA Paper 2024-2517, 2024. https://doi.org/10.2514/6.2024-2517
- [84] Hildebrand, N. J., Mysore, P., Choudhari, M., Venkatachari, B. S., and Paredes, P., "Transition Prediction of Boundary Layers in the Presence of Backward-Facing Steps," *AIAA Journal*, Vol. 60, No. 7, July 2022, pp. 4149-4169. https://doi.org/10.2514/1.J061296
- [85] Wang, Y. and Gaster, M., "Effect of Surface Steps on Boundary Layer Transition," *Experiments in Fluids*, Vol. 39, No. 4, 2005, pp. 679–686. https://doi.org/10.1007/s00348-005-1011-7
- [86] Buchta, D. A., Laurence, S. J., and Zaki, T., "Assimilation of Wall-Pressure Measurements in High-Speed Flow over a Cone," *J. Fluid Mech.*, Vol. 947, 2022, R2. https://doi.org/10.1017/jfm.2022.668 2022